

## **Trifunctional lipid probes for comprehensive studies of single lipid species in living cells**

Doris Höglinger<sup>a,b</sup>, André Nadler<sup>a,c</sup>, Per Haberkant<sup>a</sup>, Joanna Kirkpatrick<sup>a,d</sup>, Martina Schifferer<sup>a</sup>, Frank Stein<sup>a</sup>, Sebastian Hauke<sup>a</sup>, Forbes D. Porter<sup>e</sup> and Carsten Schultz<sup>a,1</sup>

<sup>a</sup> Cell Biology & Biophysics Unit, European Molecular Biology Laboratory, Meyerhofstr.1, 69117 Heidelberg, Germany

<sup>b</sup> Department of Pharmacology, University of Oxford, Mansfield Road, Oxford OX1 3QT, United Kingdom

<sup>c</sup> Max Planck Institute of Molecular Cell Biology, Pfotenhauerstr. 108, 01307 Dresden, Germany

<sup>d</sup> Leibniz Institute on Ageing – Fritz Lipmann Institute, Beutenbergstr. 11, 07745 Jena, Germany

<sup>e</sup> Eunice Kennedy Shriver National Institute of Child Health and Human Development, National Institutes of Health, Bethesda, United States

<sup>1</sup> Contact information: [schultz@embl.de](mailto:schultz@embl.de), phone: +49-6221-387-8210

**Classification:** Biological sciences (Cell biology)

**Keywords:** sphingosine, diacylglycerol, caged lipids, photoaffinity labelling, protein-lipid interaction, lipid localization, Niemann-Pick disease type C

## **ABSTRACT**

Lipid-mediated signaling events regulate many cellular processes. Investigations of the complex underlying mechanisms are difficult because several different methods need to be employed under varying conditions. Here we introduce multifunctional lipid derivatives to study lipid metabolism, lipid-protein interactions and intracellular lipid localization with a single tool per target lipid. The probes are equipped with two photoreactive groups to allow photo-liberation (uncaging) and photo-crosslinking in a sequential manner as well as a click-handle for subsequent functionalization. We demonstrate the versatility of the design for the signaling lipids sphingosine and diacylglycerol. Uncaging of the probe for these two species triggered calcium signaling and intracellular protein translocation events, respectively. We performed proteomic screens to map the lipid-interacting proteome for both lipids. Finally, we visualized a sphingosine transport deficiency in patient-derived Niemann-Pick disease type C fibroblasts by fluorescence as well as correlative light and electron microscopy, pointing towards the diagnostic potential of such tools. We envision that this type of probes will become important for analyzing and ultimately understanding lipid signaling events in a comprehensive manner.

## **SIGNIFICANCE STATEMENT (120 words max)**

Some lipids such as sphingosine and diacylglycerol are potent signaling effectors. However, comprehensive investigations of their bioactive actions are often hampered by a lack of tools that can be used in living cells. Here, we present novel, chemically modified lipids which allow to investigate acute lipid signaling, lipid metabolism, lipid-protein interactions as well as lipid localization by using a single probe for each target lipid. Equipped with a caging group, the lipid probe is biologically inactive, until activated by a flash of light. A second photoreaction crosslinks the probe to protein interactors which may subsequently be analyzed by mass spectrometry or fluorescence/electron microscopy. We envision that this versatile design will be central to unraveling complex lipid signaling networks.

\body

## INTRODUCTION

The roles of lipids in cells go far beyond providing the structural backbone of cellular membranes. Certain lipid species are powerful signaling molecules. Examples include the roles of sphingosine (Sph) and the diacylglycerol (DAG) variant, stearyl-arachidonylglycerol (SAG) in intracellular calcium signaling (1, 2). The study of such signaling lipids is often complicated by the fact that they are under tight metabolic control and that they occur only in very low concentrations. Overexpression of metabolic enzymes as a means to manipulate the levels of signaling lipids, is a slow process when compared to the rapid turnover of those lipids and may therefore produce not only the target lipid but also multiple downstream metabolites. Chemical dimerizer and optogenetic approaches are possibilities to more rapidly manipulate lipid contents, but they depend on cytosolic lipid metabolizing enzymes. Therefore in the past, many applications were focused on phosphoinositides (3, 4). A more general way to rapidly increase lipid concentration is the use of caged lipids. These are equipped with a photo-cleavable protecting group (caging group), which blocks biological activity and renders them resistant to metabolic turnover before the active lipid is released using a flash of light (2, 5–7). The sudden increase in target lipid concentration facilitates analysis of downstream lipid signaling events as well as lipid metabolism within living cells in pulse-chase experiments.

In order to correctly interpret such signaling events, underlying processes such as lipid-protein interactions, intracellular lipid localization and kinetics of lipid metabolism need to be considered. To date, lipid metabolism is typically monitored using isotope labeled or alkyne modified lipids (8–10). Fluorescent lipids, lipid binding antibodies or lipid biosensors are mainly employed to study lipid localization (11, 12). Most assays for studying lipid-protein interactions rely on reconstituted membranes/liposomes and are therefore largely restricted to soluble proteins (13–16). The plethora of methods used to investigate these different processes makes it difficult to compare or validate their respective results. A promising approach to integrate the study of lipid metabolism, lipid localization and lipid-protein interactions has emerged in recent years: bifunctional lipids feature a small diazirine group to allow photo-crosslinking with interacting proteins in the intact cellular environment and a terminal alkyne for subsequent functionalization (17). Biotinylation of crosslinked lipid-protein conjugates enables their enrichment and identification of lipid-interacting proteins. To date, bifunctional lipids are one of the few methods to screen for lipid protein interactions in living cells (18–21). Alternatively, bifunctional lipids can be used to visualize lipid localization by click-reaction with a fluorophore (1, 18, 20). The application of the bifunctional lipid principle to signaling lipids, however, is handicapped by their tight metabolic control. Any precursor is

rapidly incorporated into downstream lipids, complicating the interpretation of resulting data. The ability to liberate a single, well-defined signaling lipid species within cells and to immediately capture its interacting partners, investigate downstream signaling, and study its subcellular localization would allow much-needed insight into the regulation of lipid-dependent signaling to be gained.

Here, we present 'trifunctional' lipids as novel tools, combining the advantages of caged and bifunctional lipids in a single molecule to allow for a wide range of studies in living cells with tight temporal control. Applied to Sph and DAG, we show that trifunctional lipids enable (i) acute alteration of signaling lipid concentration, (ii) measurement of lipid metabolism both on a population-wide as well as on a single-cell level, (iii) screening for lipid-protein interactions and (iv) direct visualization of lipid localization by light and correlative light and electron microscopy (CLEM) in comparable experimental settings.

## RESULTS

**Synthesis of trifunctional sphingosine (TFS, 1), diacylglycerol (TFDAG, 2) and a trifunctional fatty acid (TFFA, 3).** The previously reported (20) bifunctional sphingosine **4** was equipped with a coumarin caging group via carbamate linkage at the amino group giving the TFS **1** in 96% yield (Figure 1a). Synthesis of TFDAG **2** started by PMB protection of the free hydroxyl group of *S*-isopropylidene glycerol followed by removal of the isopropylidene group to give diol **6**. DMT protection of the primary hydroxyl group and attachment of arachidonic acid to the secondary hydroxyl group gave intermediate **7**. The PMB-protected diacylglycerol **8** was obtained by mild DMT deprotection using FeCl<sub>3</sub> in MeOH/DCM and carbodiimide mediated coupling of the bifunctional fatty acid **9**. The PMB group was removed by brief exposure to acidic conditions at 0 °C, effectively preventing acyl migration as the alternative regioisomers were not detected by NMR. Lastly, *N,N*-diethylaminocoumarin was linked to the primary hydroxyl of **10**, giving the TFDAG **2** (Figure 1b). TFFA **3** was obtained by standard carbodiimide-mediated attachment of the coumarin group (Figure 1c).

***In vitro* validation of sequential photoreactions.** We established that the photoreactions used for uncaging and crosslinking are indeed orthogonal and may be carried out in a sequential manner. To this end, a 1 mM solution of TFDAG **2** in MeOH-d<sub>4</sub> was irradiated using a UV mercury arc source equipped with 400 nm and 355 nm highpass filters. The uncaging reaction was performed at >400 nm, while photo-crosslinking the diazirine group required 355 nm light. <sup>1</sup>H-NMR spectra were acquired after each irradiation step and compared to the spectrum of the corresponding pure compounds **2** and **10** (Figure 1d). We

found that uncaging at >400 nm quantitatively removed the coumarin group. This is indicated by signals stemming from the protons in the glycerol backbone (highlighted in blue and red), which, upon illumination give the same pattern also exhibited by the bifunctional DAG reference compound. The diazirine moiety (green signals) is unaffected by uncaging and is only activated by UV light of >355 nm. Crucially, the alkyne group remained intact through all illumination steps (cyan signals in Figure 1d), enabling subsequent functionalization.

**Uncaging of trifunctional lipids in living cells.** After establishing photochemical suitability, we applied trifunctional lipids to living cells for investigating their biocompatibility and signaling functionality. The intracellular release of Sph has recently been reported to induce cytosolic calcium increase by release from acidic stores (1) whereas elevated DAG levels trigger rapid translocation of C1-domain containing proteins to the plasma membrane (2). As expected, local uncaging of TFS led to  $\text{Ca}^{2+}$  transients for 40-80 s as measured by the cytosolic calcium dye Fluo-4. The kinetics of calcium release were comparable to previously demonstrated uncaging of native Sph (1). Importantly, the negative control compound dihydrosphingosine (dhSph) was unable to elicit calcium release under these conditions (Figure 2a, 2b). The effects of DAG elevation were monitored by the translocation of a DAG-binding C1-domain fused to GFP. When adding the bifunctional DAG probe **10** to the medium of HeLa cells expressing the DAG sensor C1-GFP, we observed translocation of the protein to the plasma membrane over the course of two minutes, indicating that the compound closely mimics the biological activity of its natural analog, SAG (Figure 2c, upper panel). Simple addition of TFDAG on the other hand failed to induce C1-GFP translocation, demonstrating its biological inertness in the caged form. Only 405 nm uncaging of TFDAG through the microscope objective induced translocation (Figure 2c, lower panel). It is important to note that illumination through the microscope objective only uncages a small fraction of the probe compared to biochemical bulk experiments which make use of strong UV lamps. The simultaneous uncaging of all probe molecules in such biochemical experiments can be used to investigate probe metabolism by thin-layer chromatography (TLC, Figure S1). Here, cells labelled with 3  $\mu\text{M}$  TFS or 50  $\mu\text{M}$  TFDAG were subjected to pulse-experiments, the resulting metabolites were visualized by click reaction (8) and separated on TLC. Unfortunately, the TFDAG probe partially fragmented into DAG and FA during lipid extraction and click reaction (Figure S1c and S1d). TFS, on the other hand, was stable in cells (Figure S1a) and upon uncaging was readily incorporated into sphingolipids as well as phospholipids (Figure S1b) in accordance with previous studies using bifunctional sphingosine (20). Together with the results obtained by live-cell microscopy, this confirms that the diazirine and alkyne moieties do not impact on the biological activity of Sph and DAG, respectively and that acute signaling events can be triggered by uncaging of trifunctional lipids.

**Quantification of DAG turnover at the plasma membrane.** Being able to trigger C1-GFP translocation to the plasma membrane in a controlled fashion allowed us quantify lipid turnover both on a population-wide as well as on a single cell level, thereby accounting for the inherent heterogeneity of cell populations. Compared to standard biochemical experiments, such live-cell uncaging experiments also offer superior temporal resolution, however they do not measure pure metabolism as the signal acquired through biosensors accounts for both lipid transport and metabolic transformations. Here, we performed a series of field-of-view uncaging experiments using TFDAG and compared it to caged SAG (2) (Supporting movies M1 and M2). To quantify changes in plasma membrane DAG levels, the ratio between plasma membrane bound and cytosolic fractions of C1-GFP were calculated using a recently developed algorithm (23) (see SI Materials and Methods for details). Most cells exhibited significant C1-GFP translocation to the plasma membrane, with similar response rates for TFDAG and SAG, respectively (TFDAG: 78 %, SAG 71 %, Figure 2d). Kinetic traces were measured for all cells (Figure S2) and responding cells were included in the kinetic analyses. Mean translocation traces (Figure 2e) showed an initial rapid increase of the C1-GFP plasma membrane / cytosol ratio, reflective of the rapid increase of DAG concentration caused by uncaging. After reaching a maximum approximately 100 s after illumination, the observed signal declined with comparable slopes for both lipids, indicating ongoing DAG turnover. To characterize their kinetics more quantitatively, we analyzed and fitted the responses on a single cell level. A simple biexponential model featuring terms for C1-GFP recruitment to the plasma membrane and DAG turnover was fitted to the individual traces (see Figure S3 and SI Materials and Methods for details). After quality control (standard error estimate below 0.06 and a positive turnover rate, see SI Materials and Methods) a set of 31 and 43 traces were obtained for SAG and TFDAG, respectively (Figure 2f). The determined half-life times for DAG turnover (Figure 2g) revealed striking differences on a cell-to-cell level, as individual cells exhibited DAG turnover rates varying over an order of magnitude. These data suggest that heterogeneity of signaling lipid turnover might be an underrated aspect in lipid signaling events.

**Chemoproteomic profiling of lipid-protein complexes.** A further application of trifunctional lipids is the systematic mapping of lipid-protein interactions by mass-spectrometry. Owing to the two orthogonal photoreactions, which enable a “release and catch” approach, trifunctional lipids allow profiling the protein interactome of single lipid species. Due to the reduced complexity of the bait compared to bifunctional lipids, this screening technology is more sensitive to low abundant lipids and should pick up scarce lipid-protein interactions. HeLa cells were labeled with 6  $\mu$ M TFS and 100  $\mu$ M TFDAG or TFFA, respectively, which resulted in comparable loading of the cells, owing to their different uptake kinetics (Figure S4). After uncaging and photoaffinity labeling, the protein-lipid

conjugates were reacted with biotin-azide using copper-catalyzed click chemistry and subsequently enriched via neutravidin beads. The preparation of peptides for proteomic analysis was performed according to a recent protocol optimized for ultrasensitive analysis of complex biological samples (24). Using this method, a total of 3263 proteins were identified. For further analysis, only proteins which were identified in both screens using either TFS or TFDAG were considered. The peptide spectral matches of these high-confidence proteins are displayed as a heat-map in Figure 3a. As noted in previous studies using bifunctional lipids (20, 21), a high overlap in the interactome of different lipids was observed. This may be attributed to unspecific crosslinking of highly abundant proteins with either probe or background binding to the beads during the pull-down procedure, highlighting the need for control lipids. By grouping the resulting proteins according to the ratio of their peptide spectral matches over control lipids, we were able to identify two subsets of proteins, which interacted preferentially with either TFS (Figure 3a, top left group) or TFDAG (bottom right group). A sample 55 hits are displayed for TFS and TFDAG, respectively. The full list of proteins arranged as in Figure 3a as well as lists for Sph- and DAG-interacting proteins can be found in Supporting Table 1. Reassuringly, we found proteins previously reported to interact with Sph (ceramide synthase 2, which uses Sph as a substrate (25) and cathepsin B, which is a mediator of Sph-induced apoptosis (26)) or with DAG (phosphatidylinositol 4,5-bisphosphate phosphodiesterase delta 3, a DAG producing enzyme (27)) among our top hits. We then compared the list of putative Sph-interacting proteins from this screen with results from a previous screen performed with bifunctional Sph (20) (Figure S5a). 14 proteins were already detected using bifunctional Sph, further strengthening them as bona fide Sph-binders. Yet, the majority of these proteins were not previously identified. Here, we benefited from the major advantage of trifunctional lipids to circumvent lipid metabolism and identify scarcer or very short-lived lipid-protein interactions. In the absence of previous proteomic screens with DAG as bait, we compared proteins identified using TFDAG to hits from previous screens performed with AEA-DA and A-DA (21). These endocannabinoid probes contain arachidonic acid just as TFDAG does. Reassuringly, only 17 of 130 putative DAG-interacting proteins were previously identified using the endocannabinoid probes (Figure S5b). This further confirms that proteins identified with TFDAG are specifically interacting with DAG.

**Subcellular localization of lipids and lipid-interacting proteins.** To further analyze these new, putative Sph and DAG-interacting proteins, we accessed their GO-terms and compared the annotated subcellular localizations of TFS and TFDAG hits (Figure 3b). A larger percentage of TFS-interactors were annotated to the secretory pathway (ER, Golgi, vesicles, endosomes, lysosomes and exosomes) compared to TFDAG hits, which are mainly annotated as cytosolic proteins. This result hints towards a different subcellular localization

of the trifunctional lipids at the time of crosslinking. Before uncaging, trifunctional lipids are indiscriminately localized to internal membranes and the cytoplasm as visualized by fluorescence of the coumarin caging group (see Figure S6a, top panel). To investigate their localization at the time of crosslinking, HeLa cells were treated in the same way as for the proteomic screens, but followed by fixing and staining of the lipid-protein complexes with Alexa488-azide (Figure 3c, Figure S6a, bottom panel). We observed that each lipid now localized to distinct cellular compartments. Strikingly, the staining of TFDAG resulted in 52 % - 59 % weaker fluorescence compared to TFS and TFFA, respectively (Figure S6b). Cytosolic and nuclear proteins are known to be extracted by methanol fixation (28), which is necessary for this protocol as it removes all non-crosslinked lipids. This may explain the reduced fluorescence intensity in these regions and confirms the GO-term analysis of DAG-interacting proteins which listed surprisingly many cytosolic proteins. We speculate that the high proportion of cytosolic proteins likely reflects a highly efficient DAG transporting machinery, which requires extraction of DAG from membranes, thereby potentially exposing the crosslinkable group. For example, extended synaptotagmins (E-Syts) were recently shown to extract DAG from the plasma membrane (29). Accordingly, we identified both E-Syt1 and E-Syt2 in screens performed with TFDAG. However, E-Syt1 was also found using TFS and TFFA and E-Syt2 was identified with TFS, but not with TFFA, hinting at a broader lipid specificity of these proteins. TFS on the other hand was found to be predominantly localized to the perinuclear ER, Golgi and, mainly, endosomes/lysosomes (see Figures S6c, S6e and S6f for co-localization). We quantified the amount of Sph-labelling in LAMP1-stained compartments to 40 % of total fluorescence whereas the more uniform labelling of TFDAG only localized 22 % of total fluorescence to areas also marked by LAMP1 (Figure S6d).

**Sphingosine localization in Niemann-Pick disease type C.** To highlight the potential of trifunctional lipids for the visualization of subcellular lipid localization, we chose as an example the study of Niemann-Pick disease type C (NPC) cells. NPC is a rare lysosomal storage disease caused mainly by mutation of the gene encoding for the NPC1 protein (30). In diseased cells, Sph is known to accumulate alongside other lipids such as sphingomyelin, cholesterol and higher glycosphingolipids (31, 32). The function of NPC1 is not fully understood, but NPC cells exhibit a trafficking defect at the late endosomal/lysosomal stage, as observed for cholesterol by using Filipin staining (33). Accumulation of Sph and lactosylceramide was previously visualized using fluorescent lipid analogues (34, 35). Here, we used TFS to visualize Sph localization and trafficking. To create a cellular model of the NPC disease, HeLa cells were either treated with the cationic amphiphilic drug U18666A, which acts as an NPC1 inhibitor (36) or with siRNA targeted to NPC1. Both treatments produced an NPC phenotype as confirmed by Filipin staining (Figure S7a). Using TFS on



these cell models, a noticeable increase of fluorescence was observed in late endosomal/lysosomal vesicles (Figure 4a, for co-localization see Figure S7b), indicative of Sph storage.

**Sphingosine transport in Niemann-Pick disease type C.** We then investigated whether the transport of Sph out of the acidic compartment was affected as well. Here, the main advantages of trifunctional lipids became obvious: by using two photoreactions (uncaging/crosslinking), it was possible to bypass the uptake and possible retention of Sph in the endocytic pathway and to set up pulse-chase experiments. The accumulation of bifunctional Sph **4** in acidic compartments after uncaging set a precise starting point for quantifying transport of Sph and its metabolites out of the acidic compartment. In control cells, Sph was rapidly (< 10 min) cleared from the vesicles as exemplified by a drop in Pearson's correlation coefficient with the late endosomal/lysosomal marker LAMP1 (Figure S7b). Both NPC models (U18666A, siRNA) on the other hand, retained most Sph in the late endosomal/lysosomal vesicles even after 30 min post-uncaging (Figure 4a) as expected for cells with lipid transport defect. Next, we investigated Sph transport in skin fibroblasts derived from three NPC patients with varying disease severity. Cells derived from the patient with the mildest phenotype were able to export most of the lysosomal Sph within 10 min, whereas the more severe patients still showed marked lysosomal Sph accumulation after 30 min (Figure 4b). We quantified this retention by investigating the skewness of the pixel distribution in each cell through automated image processing (Figure 4c). High skewness values represent vesicular staining whereas lower values are indicative of an even distribution throughout the cells as achieved by ER or internal membrane staining.

**Ultrastructural localization of sphingosine.** In order to further examine this accumulation on an ultrastructural level, we subjected NPC patient fibroblasts to high-precision correlative light-and 3D electron microscopy (CLEM). Briefly, crosslinked lipids were functionalized with Alexa594-azide followed by high-pressure freezing and thin-sectioning. Fluorescent and electron dense fiducial marker beads (37) were used to correlate fluorescence images and electron tomograms (Figure 4d). We found that Sph localized to intraluminal vesicles of late endosomes/multivesicular bodies, which strengthens the hypothesis of a trafficking block at the late endosomal stage.

## DISCUSSION

In summary, we have developed a novel photochemical probe type featuring two sequential photoreactions, which allows different aspects of lipid biology to be studied while using the same molecule. Importantly, trifunctional lipids constitute a unique way to investigate single lipid species in a live-cell setting, which is especially important when looking at active signaling lipid species. We successfully employed these probes to quantify cellular signaling

after uncaging by live-cell imaging of downstream effects including C1-domain translocation and changes of calcium levels. Trifunctional lipids have furthermore proven useful in the unbiased identification of novel, putative Sph and DAG-interacting proteins by proteomic analysis. Some of the identified, high-confidence interactors open up exciting avenues for further study: For example, we found beta-hexosaminidase A and B (HexA and HexB) to interact with Sph. It is interesting to speculate that Sph might act as regulator of lipid catabolizing enzymes such as HexA, the activity of which is known to depend on the lipid composition of the substrate membranes (38). Such a potential regulation of HexA by Sph might thereby further contribute to lipid storage diseases such as Niemann-Pick type C, which accumulate glycosphingolipids. A further application of trifunctional lipids lies in the visualization of their subcellular localization by fluorescence microscopy and CLEM. Reassuringly, the annotated cellular compartments of the identified proteins corresponded well with their observed localization. Taking this further, we set up an assay to investigate the transport of Sph in NPC disease and observed a trafficking block at the late endosomal stage. For the future, we imagine that this trafficking assay could serve as a valuable diagnostic tool complementing the established Filipin staining analysis as it is independent of cholesterol accumulation but assays the capability of the cells to move Sph out of late endosomes/lysosomes. In the three NPC cell lines investigated, this correlated well with patients' severity scores. However, further tests on a larger number of patient samples will be necessary to confirm that Sph retention in the late endosomes / lysosomes is a marker for disease severity.

In conclusion, we demonstrated the practicality of trifunctional lipids for studying different aspects of lipid biology in the context of living cells and we envision that this design will lead to the generation of more trifunctional lipids and studies of the relevant signaling networks.

## **MATERIALS AND METHODS**

**Chemical synthesis and cell culture.** Detailed protocols for the synthesis of trifunctional lipids and their characterization data can as well as information about the cell lines and their culture conditions be found in SI Materials and Methods.

**Confocal uncaging experiments.** HeLa cells were transfected with C1-GFP 24 hours prior to uncaging experiments. For calcium imaging experiments, cells were labelled with 100  $\mu$ L of 5  $\mu$ M Fluo4-AM for 30 min prior to the experiment. Cells were treated with a 100  $\mu$ M solution of the respective caged DAG (TFDAG or SAG) or a 2  $\mu$ M solution of TFS in imaging buffer and allowed to equilibrate at 37 °C for 5-10 min. Confocal time-lapses were acquired at 37 °C using an Olympus FV1200 confocal microscope with a 63x oil objective. Uncaging

was performed by either scanning the entire field of view with a 405 nm laser set to 40% laser intensity or by spot-uncaging using the tornado function of the Olympus software using the 405 nm laser line set to 50 % intensity for 3 s at 2  $\mu$ s per pixel. For more detailed protocols including excitation and emission settings as well as image analysis procedures refer to SI Materials and Methods.

**Lipid analysis by thin-layer chromatography.** Briefly, cells were labelled with 3  $\mu$ M TFS or 50  $\mu$ M TFDAG for the indicated times and subjected to UV-induced uncaging, as indicated. Cellular lipids were extracted, labelled with 3-azido-7-hydroxycoumarin via click-reaction, separated on a TLC-plate and visualized via the coumarin fluorescence.

**Proteomic screens.** A detailed procedure can be found in SI Materials and Methods. Briefly, HeLa cells were labelled with 100  $\mu$ M TFFA for 15 min, 100  $\mu$ M TFDAG for 15 min and 6  $\mu$ M TFS probe for 5 min, respectively. The cells were then UV-irradiated for 2.5 min at wavelengths >400 nm followed by a second 2.5 min irradiation at wavelengths >345 nm. The lysate was subjected to click reaction with biotin-azide and mixed with 10  $\mu$ L NeutrAvidin agarose resin. After 1 h incubation at room temperature, the resin was washed with PBS/1 % SDS and the proteins were eluted using  $\beta$ -mercaptoethanol-containing elution buffer. Proteins were digested according to a recently developed protocol (24) and subjected to high-pH fractionation (43). Peptides were separated using the nanoAcquity UPLC system coupled directly to an LTQ OrbitrapVelos Pro using the Proxeonnanospray source.

**Visualization of lipid-protein complexes in cells.** A detailed protocol for visualizing lipids in cells by fluorescent microscopy as well as by of correlated light- and electron microscopy can be found in SI Materials and Methods.

## ACKNOWLEDGEMENTS

We are grateful for the support from the Advanced Light Microscopy Facility and the Proteomic Core Facility of the European Molecular Biology Laboratory. This research has received funding from the European Union Seventh Framework Programme under grant agreement no 289278 - "Sphingonet" as well as Transregio 83 funded by the DFG. This work was partially supported by the intramural research program of NICHD, NIH. MS is a fellow of the EMBL Interdisciplinary Postdoc Program, co-funded by the EU.

## REFERENCES

1. Höglinger D, et al. (2015) Intracellular sphingosine releases calcium from lysosomes. *Elife* 4:e10616.

2. Nadler A, et al. (2013) The fatty acid composition of diacylglycerols determines local signaling patterns. *Angew Chem Int Ed Engl* 52(24):6330–6334.
3. Feng S, et al. (2014) A rapidly reversible chemical dimerizer system to study lipid signaling in living cells. *Angew Chemie - Int Ed* 53(26):6720–6723.
4. Idevall-Hagren O, Dickson E, Hille B, Toomre DK, De Camilli P (2012) Optogenetic control of phosphoinositide metabolism. *Proc Natl Acad Sci U S A* 109(35):E2316–E2323.
5. Höglinger D, Nadler A, Schultz C (2014) Caged lipids as tools for investigating cellular signaling. *Biochim Biophys Acta - Mol Cell Biol Lipids* 1841(8):1085–1096.
6. Mentel M, Laketa V, Subramanian D, Gillandt H, Schultz C (2011) Photoactivatable and cell-membrane-permeable phosphatidylinositol 3,4,5-trisphosphate. *Angew Chem Int Ed Engl* 50(16):3811–3814.
7. Hövelmann F, et al. (2016) Optotaxis: Caged Lysophosphatidic Acid Enables Optical Control of a Chemotactic Gradient. *Cell Chem Biol* 23:629–634.
8. Thiele C, et al. (2012) Tracing fatty acid metabolism by click chemistry. *ACS Chem Biol* 7(12):2004–11.
9. Matyas GR, Beck Z, Karasavvas N, Alving CR (2009) Lipid binding properties of 4E10, 2F5, and WR304 monoclonal antibodies that neutralize HIV-1. *Biochim Biophys Acta - Biomembr* 1788(3):660–665.
10. Alvarez-Vasquez F, Sims KJ, Cowart LA (2005) Simulation and validation of modelled sphingolipid metabolism in *Saccharomyces cerevisiae*. *Nature* 433(January):425–430.
11. Kuerschner L, et al. (2005) Polyene-lipids: a new tool to image lipids. *Nat Methods* 2(1):39–45.
12. Nishioka T, et al. (2008) Rapid Turnover Rate of Phosphoinositides at the Front of Migrating MDCK Cells. *Mol Biol Cell* 19:4213–4223.
13. Manifava M, et al. (2001) Differential Binding of Traffic-related Proteins to Phosphatidic Acid- or Phosphatidylinositol (4,5)-Bisphosphate-coupled Affinity Reagents. *J Biol Chem* 276(12):8987–8994.
14. Gallego O, et al. (2010) A systematic screen for protein-lipid interactions in *Saccharomyces cerevisiae*. *Mol Syst Biol* 6(430):430.
15. Saliba A-E, et al. (2014) A quantitative liposome microarray to systematically

- characterize protein-lipid interactions. *Nat Methods* 11(1):47–50.
16. Ceccato L, et al. (2016) PLIF : A rapid , accurate method to detect and quantitatively assess protein-lipid interactions. 9(421):1–10.
  17. Haberkant P, Holthuis JCM (2014) Fat & fabulous: Bifunctional lipids in the spotlight. *Biochim Biophys Acta*. doi:10.1016/j.bbalip.2014.01.003.
  18. Haberkant P, et al. (2013) In vivo profiling and visualization of cellular protein-lipid interactions using bifunctional fatty acids. *Angew Chem Int Ed Engl* 52(14):4033–8.
  19. Hulce JJ, Cognetta AB, Niphakis MJ, Tully SE, Cravatt BF (2013) Proteome-wide mapping of cholesterol-interacting proteins in mammalian cells. *Nat Methods* 10(3):259–64.
  20. Haberkant P, et al. (2015) Bifunctional Sphingosine for Cell-Based Analysis of Protein-Sphingolipid Interactions. *ACS Chem Biol*. 11, 222-30.
  21. Niphakis MJ, et al. (2015) A Global Map of Lipid-Binding Proteins and Their Ligandability in Cells. *Cell* 161(7):1668–1680.
  23. Nadler A, et al. (2015) Exclusive photorelease of signalling lipids at the plasma membrane. *Nat Commun* 6(May):10056.
  24. Hughes CS, et al. (2014) Ultrasensitive proteome analysis using paramagnetic bead technology. *Mol Syst Biol* 10(757):1–14.
  25. Levy M, Futerman AH (2010) Mammalian ceramide synthases. *IUBMB Life* 62(5):347–356.
  26. Kågedal K, Zhao M, Svensson I, Brunk UT (2001) Sphingosine-induced apoptosis is dependent on lysosomal proteases. *Biochem J* 359(Pt 2):335–343.
  27. Pawelczyk T, Matecki A (1999) Phospholipase C-d3 binds with high specificity to phosphatidylinositol 4,5-bisphosphate and phosphatidic acid in bilayer membranes. *Eur J Biochem* 262(2):291–298.
  28. Hoetelmans RW, et al. (2001) Effects of acetone, methanol, or paraformaldehyde on cellular structure, visualized by reflection contrast microscopy and transmission and scanning electron microscopy. *Appl Immunohistochem Mol Morphol* 9(4):346–351.
  29. Saheki Y, et al. (2016) Control of plasma membrane lipid homeostasis by the extended synaptotagmins. *Nat Cell Biol* 18(5):504–515.
  30. Vanier MT (2010) Niemann-Pick disease type C. *Orphanet J Rare Dis* 5:16.

31. te Vruchte D, et al. (2004) Accumulation of glycosphingolipids in Niemann-Pick C disease disrupts endosomal transport. *J Biol Chem* 279(25):26167–75.
32. Lloyd-Evans E, et al. (2008) Niemann-Pick disease type C1 is a sphingosine storage disease that causes deregulation of lysosomal calcium. *Nat Med* 14(11):1247–55.
33. Sokol J, et al. (1988) Type C Niemann-Pick disease Lysosomal accumulation and defective intracellular mobilization of low density lipoprotein cholesterol. *J Biol Chem* 263(7):3411–3417.
34. Sun X, et al. (2001) Niemann-Pick C Variant Detection by Altered Sphingolipid Trafficking and Correlation with Mutations within a Specific Domain of NPC1. 1361–1372.
35. Blom T, Li Z, Bittman R, Somerharju P, Ikonen E (2012) Tracking sphingosine metabolism and transport in sphingolipidoses: NPC1 deficiency as a test case. *Traffic* 13(9):1234–43.
36. Lu F, et al. (2015) Identification of NPC1 as the target of U18666A , an inhibitor of lysosomal cholesterol export and Ebola infection. *Elife* 4:1–16.
37. Kukulski W, et al. (2011) Correlated fluorescence and 3D electron microscopy with high sensitivity and spatial precision. *J Cell Biol* 192(1):111–119.
38. Sandhoff K (2016) Neuronal sphingolipidoses: Membrane lipids and sphingolipid activator proteins regulate lysosomal sphingolipid catabolism. *Biochimie*: doi: 10.1016/j.biochi.2016.05.004.
39. Shimada Y, Usuda K, Okabe H, Suzuki T, Matsumoto K (2009) Deracemization of 1,2-diol monotosylate derivatives by a combination of enzymatic hydrolysis with the Mitsunobu inversion using polymer-bound triphenylphosphine. *Tetrahedron Asymmetry* 20(24):2802–2808.
40. Sato S, et al. (2012) Occurrence of a bacterial membrane microdomain at the cell division site enriched in phospholipids with polyunsaturated hydrocarbon chains. *J Biol Chem* 287(29):24113–24121.
41. Stein F, Kress M, Reither S, Piljic A, Schultz C (2013) FluoQ : A Tool for Rapid Analysis of Multiparameter Fluorescence Imaging Data Applied to Oscillatory Events. *ACS Chem Biol* (8):1862–1868.
42. Wickham (2009) *ggplot2: Elegant Graphics for Data Analysis* (Springer New York) Available at: <http://ggplot2.org>.

43. Bock T, et al. (2014) An integrated approach for genome annotation of the eukaryotic thermophile *Chaetomium thermophilum*. *Nucleic Acids Res* 42(22):13525–13533.
44. Smedley D, et al. (2015) The BioMart community portal: an innovative alternative to large, centralized data repositories. *Nucleic Acids Res*:1–10.
45. Avinoam O, Schorb M, Beese CJ, Briggs JAG, Kaksonen M (2015) Endocytic sites mature by continuous bending and remodeling of the clathrin coat. *Science* 348(6241):1369–72.
46. Kukulski W, et al. (2012) Precise, Correlated Fluorescence Microscopy and Electron Tomography of Lowicryl Sections Using Fluorescent Fiducial Markers *Methods Cell Biol.* 111:235-57 doi:10.1016/B978-0-12-416026-2.00013-3.
47. Kremer JR, Mastronarde DN, McIntosh JR (1996) Computer Visualization of Three-Dimensional Image Data Using IMOD. *J Struct Biol* 116:71–76.

## FIGURE LEGENDS

**Figure 1.** Synthesis of trifunctional lipids **1-3** equipped with a photocage, a crosslinkable diaziridine group and an alkyne. a) Synthesis of trifunctional sphingosine (TFS, **1**). b) Synthesis of trifunctional diacylglycerol (TFDAG, **2**). c) Synthesis trifunctional fatty acid (TFFA, **3**). d) Aliphatic section of the  $^1\text{H}$ -NMR spectrum of the TFDAG Glycerol  $\text{CH}_2$ -groups are labeled red and blue, the  $\text{CH}_2$  groups next to the diazirine group (green) and the signals corresponding to the alkyne group (cyan). Samples were irradiated for 2 min with  $>400$  nm and for 2 min with  $>355$  nm light. The latter reaction produces a ketone. A spectrum of pure bifunctional DAG (BFDAG, **10**, bottom) is shown for comparison.

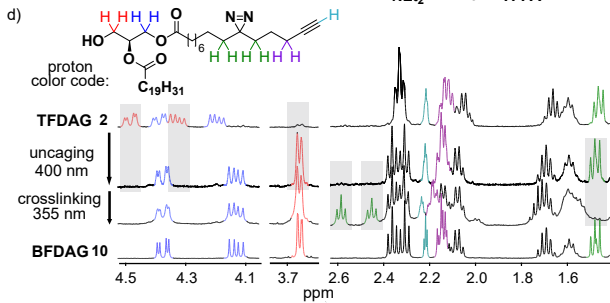
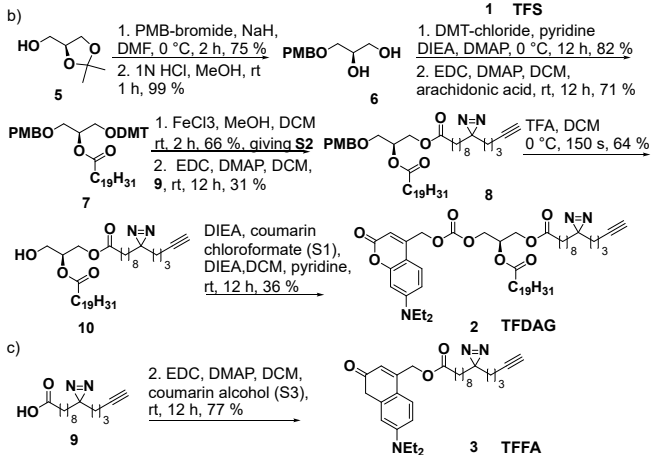
**Figure 2.** Trifunctional lipids for the study of cellular signaling. a) Time-lapse confocal microscopy images of HeLa cells labelled with Fluo-4 (a cytosolic calcium indicator) and 2  $\mu\text{M}$  TFS **1**. Uncaging was performed by irradiation of a circular area within the cells (indicated by the white circle) for 3 s at  $t = 10$  s. b) Quantification of mean Fluo-4 fluorescence of cells loaded with 2  $\mu\text{M}$  caged Sph, 2  $\mu\text{M}$  caged dihydro-Sph or 2  $\mu\text{M}$  TFS, respectively. Traces represent mean values with the standard error of the mean plotted as error bars. c) Time-lapse montage of HeLa cells expressing C1-GFP and treated with 100  $\mu\text{M}$  bifunctional SAG (BFDAG) **10** at  $t=0:30$  min (upper panel) or treated with 100  $\mu\text{M}$  TFDAG **2** at  $t=0:30$  min and uncaged by scanning the entire field of view with a 405 nm laser once at  $t=4:00$  min (lower panel). d) Response rates for C1-GFP translocation upon SAG and TFDAG uncaging. e) Mean translocation traces for SAG and TFDAG uncaging with standard error of the mean plotted as error bars. f) Individual traces after a quality control step with a representative trace and the corresponding biexponential fit highlighted. g) Single cell half-life times for DAG turnover for SAG and TFDAG, respectively.

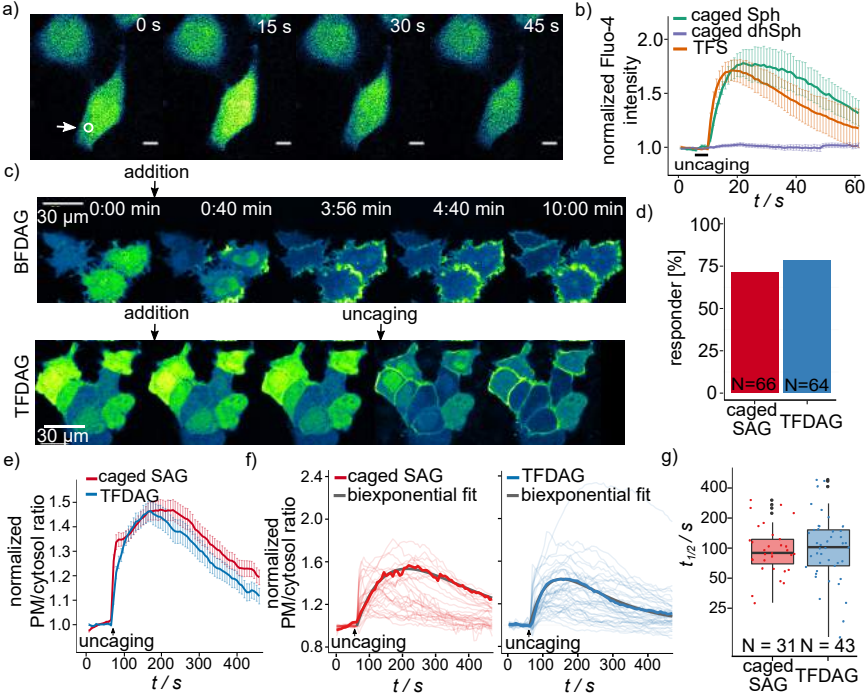
**Figure 3.** Mass spectrometric identification of Sph- and SAG-binding proteins. a) Heatmap of high-confidence proteins identified in both screens. Peptide spectral matches are color-coded according to the legend on the top. Proteins are arranged such that preferential TFS-interactors are displayed on the top (the gene symbols for the first 55 proteins are displayed on the left) and TFDAG interactor are grouped near the bottom (55 proteins are displayed on the right). b) Putative Sph- and DAG-binding were analyzed according to their cellular compartment (CC)-GO-terms. c) Confocal microscopy images of HeLa cells labelled with TFS and TFDAG, respectively, under the conditions used in the proteomic experiments. Cells were fixed with methanol, not-crosslinked lipids were washed away and the remaining crosslinked lipids were clicked to Alexa488-azide.

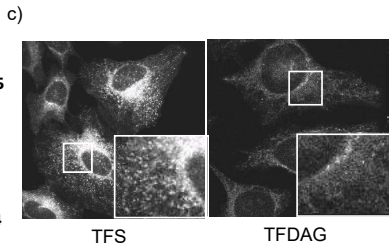
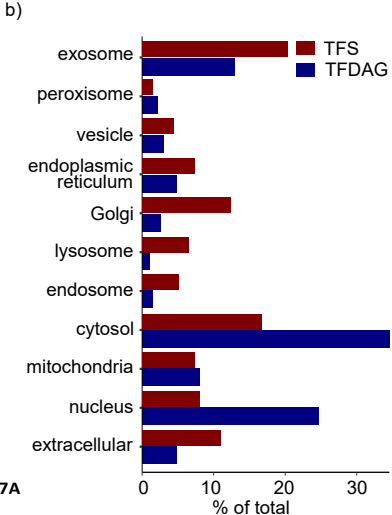
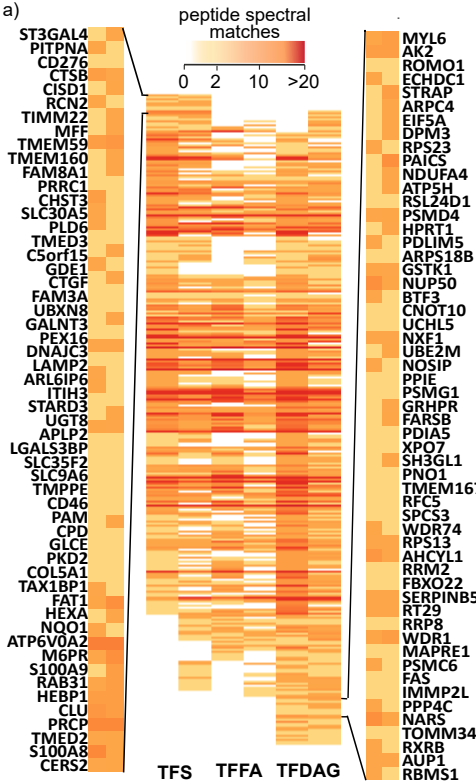
**Figure 4.** Sph localization and transport in NPC models. a) Confocal images of Sph stained with Alexa488-azide in HeLa cells in control conditions or upon induction of the NPC cellular phenotype by U18666A (2  $\mu\text{g}/\text{ml}$  for 24h) or by siRNA-mediated knockdown of NPC1. Pulse-chase experiments were performed by varying the time between uncaging and crosslinking from 0 min – 30 min. b) Confocal images of Sph stained with Alexa488-azide in human fibroblasts derived from a healthy donor (control) or from NPC patients with varying genotypes and severity scores (NPC22, NPC17, NPC25). Pulse-chase experiments were performed as in a). c) Quantification of human fibroblasts by automated image analysis. Skewness values for each cell were extracted and plotted according to cell line and time after uncaging. d) Workflow for correlative light- and electron microscopy of NPC fibroblasts.



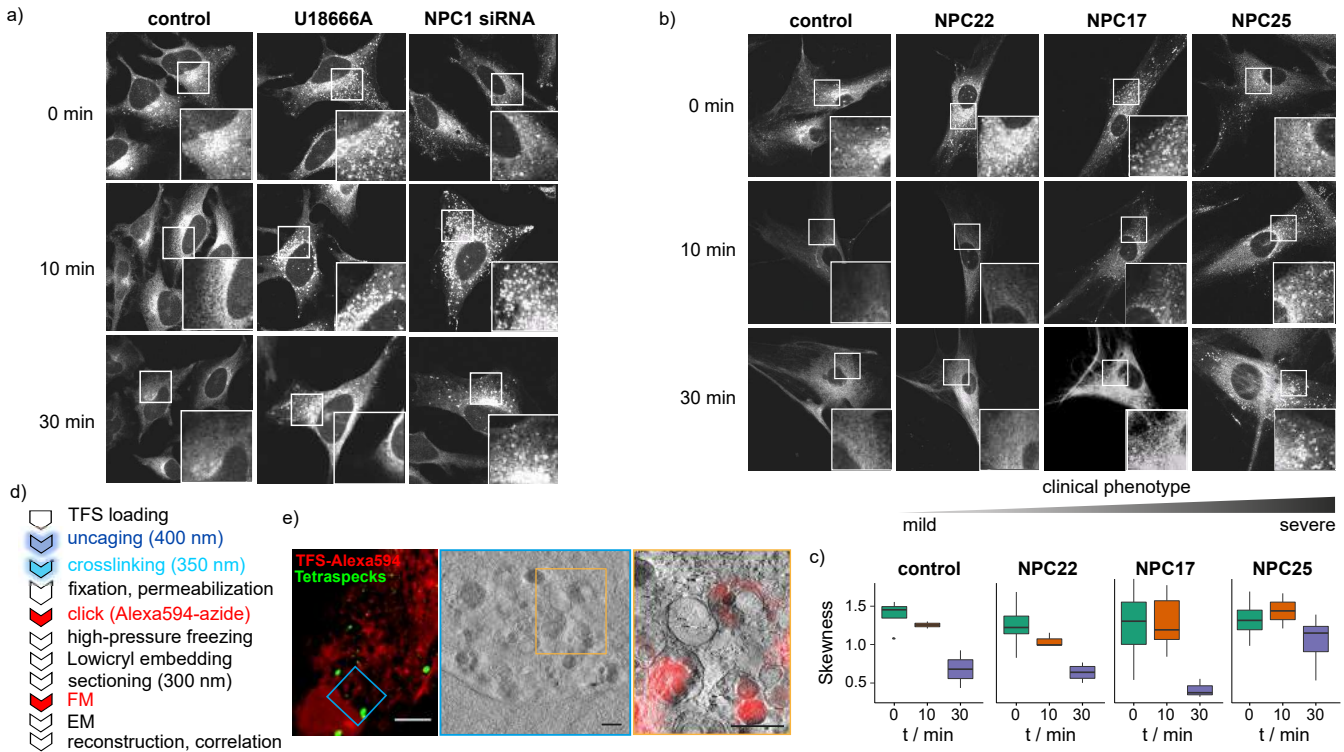
FM fluorescence microscopy, EM electron microscopy. e) CLEM images of NPC fibroblast labelled with TFS according to the procedure in d).







MYL6  
AK2  
ROMO1  
ECHDC1  
STRAP  
ARPC4  
EIF5A  
DPM3  
RPS23  
PAICS  
NDUFA4  
ATP5H  
RSL24D1  
PSMD4  
HPRT1  
PDLIM5  
ARPS18B  
GSKT1  
NUP50  
BTF3  
CNOT10  
UCHL5  
NXF1  
UBE2M  
NOSIP  
PPIE  
PSMG1  
GRHPR  
FARSB  
PDIA5  
XPO7  
SH3GL1  
PNO1  
TMEM167A  
RFC5  
SPCS3  
WDR74  
RPS13  
AHCYL1  
RRM2  
FBXO22  
SERPINB5  
RT29  
RRP8  
WDR1  
MAPRE1  
PSMC6  
FAS  
IMMP2L  
PPP4C  
NARS  
TOMM34  
RXRB  
AUP1  
RBMS1



## SUPPORTING INFORMATION

### Materials and Methods

The chemicals used were purchased from commercial sources (Acros, Sigma, Aldrich, Enzo, Lancaster or Merck) at the highest available grade and were used without further purification. Solvents for chromatography (HPLC grade) were obtained from VWR and dry solvents were obtained from Sigma. Deuterated solvents were purchased from Deutero (Karlsruhe, DE). Alexa488-azide and Alexa694-azide were obtained from Life Technologies (Thermo Fisher Scientific, Waltham, USA) and 3-azido-7-hydroxycoumarin from baseclick (#BCFA-047-1). Biotin-azide was purchased from Sigma (#762024), Neutravidin-agarose from Life Technologies (#29204). The protease inhibitor cocktail tablets were obtained from Roche (#11873580001).

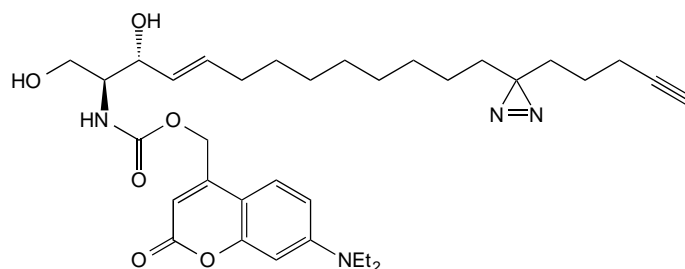
### Chemical synthesis

#### General synthetic procedures

Reaction monitoring was performed via thin layer chromatography (TLC) on plates of silica gel (Merck, 60 F254) and visualized under UV light (254 nm or 366 nm) or using a solution of phosphomolybdic acid in EtOH (10 % w/v). Preparative column chromatography was carried out using Merck silica gel 60 (grain size 0.063- 0.200 mm) under pressure (< 1.5 bar). <sup>1</sup>H-NMR and <sup>13</sup>C-NMR spectroscopy was performed on a 400 MHz Bruker UltraShield™ spectrometer at 25°C. Chemical shifts are given in ppm, referenced to the residual solvent peak. J values are given in Hz and splitting patterns are designated using s (single), d (doublet), t (triplet), q (quartet), m (multiplet) and b (broad signal). High-resolution mass spectra were recorded on a Finnigan LCQ quadrupole ion trap at the Organic Chemistry Institute and the Institute of Pharmacy and Molecular Biotechnology of the University of Heidelberg.

Compounds **4**, **6**, **9**, **S1** and **S3** as well as caged SAG were synthesized according to literature (2, 20, 39, 18). Compound **6** was equipped with a DMT protecting group using a procedure described by Sato et al (40). Detailed procedures for the synthesis of all other new compounds are given below.

(2S,3R,E)-2-amino-(7'-(diethylamino)-coumarin-4'-yl)-methoxycarbonyl)-13-(3-(pent-4'-yn-1'-yl)-3H-diazirin-3-yl)tridec-4-ene-1,3-diol (1, TFS)



A solution of 7-diethylamino-4-hydroxymethylene-coumarin (48 mg, 194  $\mu\text{mol}$ ) in 2 mL dry THF was cooled to 0 °C. DIPEA (0.1  $\mu\text{L}$ , 575  $\mu\text{mol}$ ) and phosgene (300  $\mu\text{L}$ , 610  $\mu\text{mol}$ ) were added dropwise and stirred in the dark for 2 h at 0 °C. The reaction mixture was extracted with EtOAc/H<sub>2</sub>O (1:1, 75 mL), the layers were separated, the organic layer was washed with brine and dried using Na<sub>2</sub>SO<sub>4</sub>. The solvent was removed under reduced pressure and the resulting [7-(diethylamino)-coumarin-4-yl]-methyl chloroformate was immediately used without further purification.

52  $\mu\text{L}$  DIPEA (0.3 mmol) was added to a solution of 20 mg (59.7  $\mu\text{mol}$ ) photoactivatable and clickable sphingosine (20) in 1.5 mL THF, cooled to 0 °C. [7-(diethylamino)-coumarin-4-yl]-methyl chloroformate (28 mg, 0.09 mmol) in 1 mL dry THF was added and stirred at room temperature for 1 h. The product was extracted with 30 mL EtOAc and 30 mL citric acid (5 % w/v) and washed twice with 30 mL citric acid, once with NaHCO<sub>3</sub> and once with brine. The organic phase was dried over Na<sub>2</sub>SO<sub>4</sub> and the solvent was removed under reduced pressure. The residue was purified by flash chromatography (first column: eluent: cyclohexane/EtOAc 1:1, second column: eluent: DCM/MeOH 14:1) which gave the title compound as a yellow oil (35 mg, 57.5  $\mu\text{mol}$ , 96 % yield).

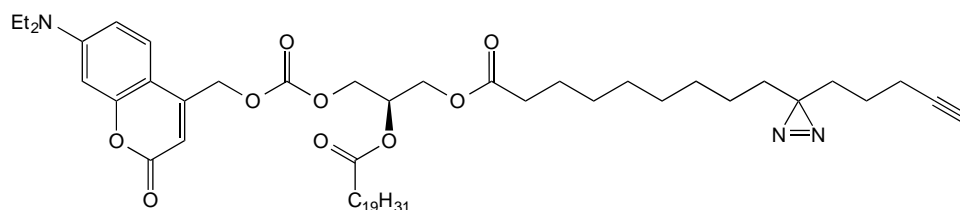
<sup>1</sup>H NMR (500 MHz, CDCl<sub>3</sub>)  $\delta$  = 7.29 (d,  $J$ =9.0, 1H), 6.58 (dd,  $J$ =8.9, 2.2, 1H), 6.50 (d,  $J$ =2.2, 1H), 6.14 (s, 1H), 5.89 (d,  $J$ =6.8, 1H), 5.84 – 5.75 (m, 1H), 5.55 (dd,  $J$ =15.2, 6.1, 1H), 5.23 (s, 2H), 4.39 (s, 1H), 4.02 (dd,  $J$ =11.2, 2.8, 1H), 3.77 (dd,  $J$ =11.5, 3.0, 1H), 3.69 (dd,  $J$ =7.8, 3.3, 1H), 3.66 – 3.59 (m, 1H), 3.41 (q,  $J$ =7.0, 4H), 2.56 (s, 2H), 2.15 (td,  $J$ =6.9, 2.6, 2H), 2.05 (dd,  $J$ =13.9, 7.0, 3H), 1.94 (t,  $J$ =2.6, 1H), 1.48 (dd,  $J$ =9.1, 6.6, 3H), 1.39 – 1.29 (m, 9H), 1.28 – 1.15 (m, 28H), 1.10 – 1.02 (m, 5H), 0.91 – 0.77 (m, 4H)

<sup>13</sup>C NMR (126 MHz, CDCl<sub>3</sub>)  $\delta$  = 162.34, 156.17, 155.63, 150.63, 134.39, 128.68, 124.40, 108.87, 105.92, 97.91, 83.49, 77.28, 77.03, 76.77, 74.72, 68.88, 62.12, 61.88, 55.67, 44.83,

32.85, 32.24, 31.85, 29.71, 29.31, 29.28, 29.17, 29.10, 29.02, 28.46, 23.81, 22.77, 17.97, 14.12, 12.43.

HRMS (m/z) calculated for  $C_{34}H_{49}N_4O_6^+$ : 609.36521, found: 609.36508

2-O-Arachidonyl-3-O-(7-(diethylamino)-coumarin-4-yl)-methoxycarbonyl-1-O-(3'(4''-pentyn-1''-yl)-H-diazirine-3'-octanoyl)-sn-glycerol (**2**, TFDAG)



A solution of **10** (55 mg, 90  $\mu$ mol, 1.0 eq.) in a mixture of dry DCM and dry pyridine (4:1, 2 ml) was subsequently treated with DIEA (0.08 ml, 816  $\mu$ mol, 9.0 eq) and a solution of freshly prepared coumarin chloroformate(2) **S1** in DCM (2 ml) at 0 °C under inert conditions. Stirring was continued and the reaction mixture was allowed to reach rt overnight. The reaction mixture was then poured into a mixture of EtOAc (100 ml) and H<sub>2</sub>O and the layers were separated. The organic layer was washed with brine (100 ml) and dried over Na<sub>2</sub>SO<sub>4</sub>. The solvent was removed under reduced pressure and the residue was purified by repeated FC (1. eluent: CyHex/EtOAc 4:1; 2. Eluent DCM/acetone 97:3) and the title compound obtained as yellow oil (28 mg, 32  $\mu$ mol, 36 %).

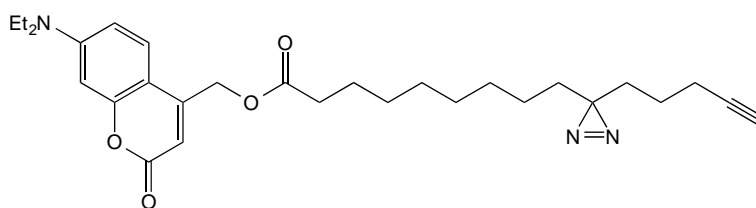
<sup>1</sup>H NMR (400 MHz, CDCl<sub>3</sub>)  $\delta$  = 7.28 (d,  $J$ =8.8, 1H), 6.58 (dd,  $J$ =9.0, 2.0, 1H), 6.51 (d,  $J$ =2.0, 1H), 6.15 (s, 1H), 5.45 – 5.24 (m, 11H), 4.42 (dd,  $J$ =11.7, 3.8, 1H), 4.37 – 4.26 (m, 2H), 4.18 (dd,  $J$ =12.0, 5.6, 1H), 3.41 (q,  $J$ =7.1, 4H), 2.86 – 2.76 (m,  $J$ =11.3, 5.5, 6H), 2.39 – 2.28 (m, 4H), 2.19 – 2.00 (m, 6H), 1.95 (t,  $J$ =2.3, 1H), 1.76 – 1.65 (m, 2H), 1.64 – 1.55 (m, 4H), 1.53 – 1.45 (m, 2H), 1.40 – 1.16 (m, 22H), 1.12 – 1.02 (m,  $J$ =7.3, 2H), 0.88 (t,  $J$ =6.7, 3H) ppm.

<sup>13</sup>C NMR (101 MHz, CDCl<sub>3</sub>)  $\delta$  = 173.18, 172.66, 161.64, 156.32, 154.42, 150.72, 148.36, 130.50, 128.99, 128.79, 128.60, 128.28, 128.12, 127.86, 127.54, 124.36, 108.72, 106.77, 105.76, 97.90, 68.89, 68.63, 66.34, 65.00, 61.62, 44.79, 33.96, 33.52, 32.83, 31.82, 31.52, 29.33, 29.19, 29.12, 29.08, 29.02, 27.22, 26.46, 25.62, 24.77, 24.68, 23.80, 22.75, 22.58, 17.96, 14.09, 12.43 ppm. Signals at 29.4-29.0 ppm are partially not resolved due to very similar <sup>13</sup>C chemical shifts.

HRMS (m/z): [M+H]<sup>+</sup> calc. for: C<sub>53</sub>H<sub>76</sub>N<sub>3</sub>O<sub>9</sub>, 898.55761, found: 898.55777



7-(diethylamino)-coumarin-4-yl)-3-(4'-pentyn-1'-yl)-H-diazirine-3-octanoate (**3**, TFFA)



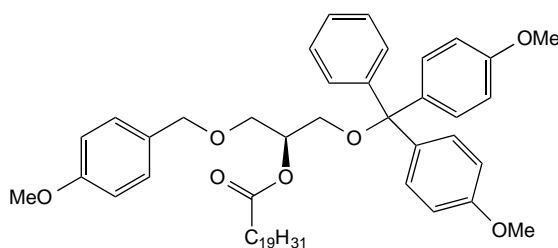
A solution of **9** (100 mg, 348  $\mu$ mol) in a mixture of EDC (0.14 g, 731  $\mu$ mol) and DMAP (6.38 mg, 62.2  $\mu$ mol) in dry DCM was treated with a solution of coumarin alcohol (89.31 mg, 382.8  $\mu$ mol) in DCM under inert conditions. The reaction mixture was stirred at 0°C for 20 min and allowed to reach room temperature overnight. The reaction mixture was then poured into a mixture of EtOAc (150 ml) and H<sub>2</sub>O and the layers were separated. The organic layer was washed with brine (150 ml) and dried over Na<sub>2</sub>SO<sub>4</sub>. The solvent was removed under reduced pressure and the residue was purified by repeated FC (1. eluent: CyHex/EtOAc 9:1; 2. Eluent CyHex/EtOAc 3:1). The title compound was obtained as yellow oil. (0.17 g, 344.6  $\mu$ mol, 97%).

<sup>1</sup>H-NMR (400 MHz, CDCl<sub>3</sub>)  $\delta$  7.29 (d,  $J$  = 9.0 Hz, 1H), 6.58 (dd,  $J$  = 9.0, 2.6 Hz, 1H), 6.52 (d,  $J$  = 2.6 Hz, 1H), 6.13 (s, 1H), 5.22 (s, 2H), 3.41 (q,  $J$  = 7.1 Hz, 4H), 2.43 (t,  $J$  = 7.5 Hz, 2H), 2.16 (td,  $J$  = 6.9, 2.6 Hz, 2H), 1.94 (t,  $J$  = 2.6 Hz, 1H), 1.73 – 1.60 (m,  $J$  = 7.3 Hz, 2H), 1.52 – 1.45 (m, 2H), 1.42 (s, 4H), 1.39 – 1.16 (m, 1H), 1.12 – 1.02 (m,  $J$  = 7.3 Hz, 2H)

<sup>13</sup>C-NMR (100 MHz, CDCl<sub>3</sub>)  $\delta$  = 206.87, 172.99, 161.83, 156.24, 150.62, 149.57, 129.00, 128.20, 125.27, 124.39, 108.67, 106.43, 106.07, 97.86, 83.45, 68.88, 61.14, 44.77, 34.08, 32.82, 31.81, 30.90, 29.15, 24.81, 23.77, 22.75, 17.94, 12.42.

HRMS (m/z): [M+H]<sup>+</sup> calc. for: C<sub>29</sub>H<sub>39</sub>N<sub>3</sub>NaO<sub>4</sub>, 516.28328; found: 516.28345.

2-O-Arachidonyl-1-O-dimethoxytrityl-3-O-(4'-methoxybenzyl)-sn-glycerol (**7**)



A solution of EDC (2.00 g, 10.4 mmol, 1.78 eq.) and DMAP (200 mg, 1.64 mmol, 0.3 eq.) in dry DCM (15 ml) was treated with arachidonic acid (2.00 g) and stirred for 10 min under inert conditions. A solution of 1-O-dimethoxytrityl-3-O-(4'-methoxybenzyl)-sn-glycerol (3.00 g, 5.84 mmol, 1.0 eq.) in dry DCM (8 ml) was added slowly and the reaction mixture stirred at rt for

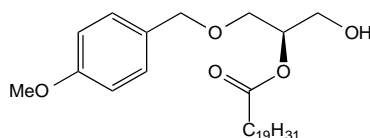
additional 3.5 h. The reaction mixture was transferred onto a mixture of EtOAc (200 ml), water (100 ml) and brine (100 ml). The layers were separated and the organic layer was washed with brine (100 ml) and dried over Na<sub>2</sub>SO<sub>4</sub>. The solvent was removed under reduced pressure and the residue purified by FC (eluent: CyHex/EtOAc 4:1). The title compound was obtained as colorless oil (3.30 g, 4.12 mmol, 71 %).

<sup>1</sup>H NMR (400 MHz, CDCl<sub>3</sub>) δ = 7.44 – 7.39 (m, 1H), 7.34 – 7.14 (m, 10H), 6.92 – 6.78 (m, 6H), 5.46 – 5.30 (m, 8H), 5.25 (m, 1H), 5.09 – 4.99 (m, 1H), 4.54 – 4.38 (m, 2H), 3.86 – 3.76 (m, 11H), 3.68 – 3.58 (m, 2H), 2.88 – 2.77 (m, 6H), 2.37 (t, *J*=6.8, 2H), 2.17 – 2.02 (m, 4H), 1.78 – 1.67 (m, 2H), 1.40 – 1.24 (m, 6H), 0.95 – 0.85 (m, *J*=1.7, 3H) ppm. Broadened signals observed, potentially two conformers in equilibrium. Cleavage of the DMT group in the next step removed this issue.

<sup>13</sup>C NMR (100 MHz, CDCl<sub>3</sub>) δ = 173.00, 158.46, 147.34, 144.83, 139.48, 135.98, 130.53, 130.50, 130.05, 129.37, 129.22, 129.15, 129.02, 128.95, 128.89, 128.84, 128.62, 128.59, 128.28, 128.24, 128.20, 128.14, 127.90, 127.87, 127.78, 127.57, 127.09, 126.74, 113.89, 113.74, 113.18, 113.07, 85.91, 73.13, 73.03, 72.75, 71.74, 68.73, 68.52, 62.81, 62.31, 55.19, 33.94, 33.75, 31.53, 29.34, 27.23, 26.93, 26.62, 26.53, 25.63, 24.90, 24.80, 22.59, 14.09 ppm. Signals at 130.5-127.5 and 27-25 ppm are partially not resolved due to very similar <sup>13</sup>C chemical shifts. Signal duplications in the glycerol and aromatic region observed. Cleavage of the DMT group in the next step removed this issue.

HRMS (*m/z*): [M+Na]<sup>+</sup> calc. for: C<sub>52</sub>H<sub>64</sub>NaO<sub>7</sub>, 823.45443, found: 823.45465.

#### 2-O-Arachidonyl-3-O-(4'-methoxybenzyl)-*sn*-glycerol (**S2**)



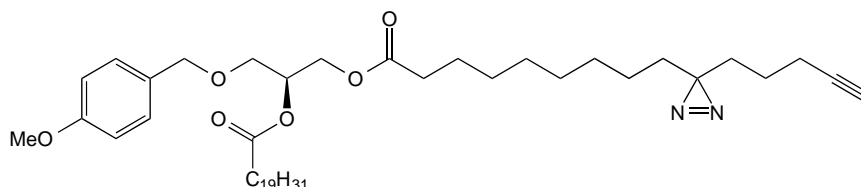
A freshly prepared solution of FeCl<sub>3</sub> (5mM) in MeOH/DCM (3:1, 20 ml) was used to dissolve **7** (950 mg, 1.19 mmol). The reaction mixture was stirred at rt for 2 h and subsequently transferred onto a mixture of H<sub>2</sub>O and EtOAc (1:1, 200 ml). The organic layer was washed with brine, dried over Na<sub>2</sub>SO<sub>4</sub> and the solvent removed under reduced pressure. The residue was purified by FC (eluent: CyHex/EtOAc 4:1) and the title compound obtained as colorless oil (383 mg, 769 μmol, 66 %, repeated twice, average yield given).

<sup>1</sup>H NMR (400 MHz, CDCl<sub>3</sub>) δ = 7.24 (d, *J*=8.6, 2H), 6.88 (d, *J*=8.6, 2H), 5.44 – 5.30 (m, 8H), 5.03 (p, *J*=4.8, 1H), 4.48 (q, *J*=11.7, 1H), 3.83 – 3.78 (m, 5H), 3.68 – 3.58 (m, 2H), 2.88 – 2.76 (m, 6H), 2.37 (t, *J*=7.6, 2H), 2.15-2.00 (m, 4H), 1.71 (p, *J*=7.5, 2H), 1.40 – 1.23 (m, 6H), 0.89 (t, *J*=6.8, 3H) ppm.

$^{13}\text{C}$  NMR (101 MHz,  $\text{CDCl}_3$ )  $\delta$  = 173.44, 159.38, 130.52, 129.68, 129.37, 128.95, 128.88, 128.61, 128.28, 128.15, 127.87, 127.54, 113.88, 73.12, 73.03, 68.71, 62.79, 55.28, 33.74, 31.53, 29.33, 27.23, 26.52, 25.62, 24.79, 22.59, 14.09 ppm.

HRMS  $[\text{M}+\text{Na}]^+$  calc. for:  $\text{C}_{31}\text{H}_{46}\text{NaO}_5$ , 521.3243, found: 521.3237.

2-O-Arachidonyl-1-O-(3'(4''-pentyn-1''-yl)-H-diazirine-3'-octanoyl)-3-O-(4'-methoxybenzyl)-sn-glycerol (8)



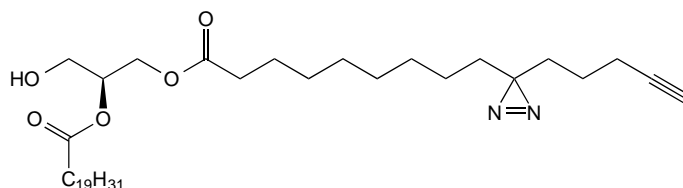
A solution of **9** (250 mg, 1.00 mmol, 1.0 eq.), EDC (300 mg, 1.56 mmol, 1.6 eq.) and DMAP (50 mg, 409  $\mu\text{mol}$ , 0.4 eq.) in dry DCM was stirred for 10 min under inert conditions. A solution of compound **8** (500 mg, 1.00 mmol, 1.0 eq) was added subsequently and stirring was continued for additional 4 h. The reaction mixture was transferred onto a mixture of water (50 ml), brine (50 ml) and EtOAc (100 ml), the layers were separated, the organic layer washed with brine (100 ml) and dried over  $\text{Na}_2\text{SO}_4$ . The solvent was removed under reduced pressure and the residue was purified by FC (eluent: CyHex/EtOAc 9:1) and the title compound obtained as colorless oil (230 mg, 314  $\mu\text{mol}$ , 31 %).

$^1\text{H}$  NMR (400 MHz,  $\text{CDCl}_3$ )  $\delta$  = 7.23 (d,  $J=8.5$ , 2H), 6.87 (d,  $J=8.5$ , 2H), 5.44 – 5.29 (m, 8H), 5.26 – 5.19 (m, 1H), 4.53 – 4.41 (m,  $J=11.7$ , 2H), 4.33 (dd,  $J=11.9$ , 3.8, 1H), 4.17 (dd,  $J=11.9$ , 6.4, 1H), 3.81 (s, 3H), 3.58 – 3.52 (m, 2H), 2.82 (dt,  $J=9.1$ , 5.2, 6H), 2.34 (t,  $J=7.6$ , 2H), 2.26 (t,  $J=7.5$ , 2H), 2.20 – 2.01 (m,  $J=30.5$ , 14.0, 4.8, 6H), 1.95 (t,  $J=2.6$ , 1H), 1.70 (p,  $J=7.5$ , 2H), 1.63 – 1.53 (m, 2H), 1.49 (dd,  $J=9.3$ , 6.5, 2H), 1.40 – 1.17 (m, 16H), 1.13 – 1.02 (m,  $J=7.8$ , 2H), 0.89 (t,  $J=6.8$ , 3H).

$^{13}\text{C}$  NMR (101 MHz,  $\text{CDCl}_3$ )  $\delta$  = 173.38, 172.88, 159.27, 130.52, 129.73, 129.33, 128.91, 128.89, 128.61, 128.27, 128.14, 127.86, 127.54, 113.82, 72.97, 70.12, 68.90, 67.86, 62.71, 55.28, 34.05, 33.71, 32.83, 31.82, 31.53, 29.34, 29.21, 29.14, 29.11, 29.04, 27.23, 26.51, 25.61, 24.81, 23.82, 22.75, 22.59, 17.96, 14.10 ppm. Signals at 29.4-29.0 ppm are partially not resolved due to very similar  $^{13}\text{C}$  chemical shifts.

HRMS (m/z):  $[\text{M}+\text{Na}]^+$  calc. for:  $\text{C}_{46}\text{H}_{68}\text{N}_2\text{NaO}_6$ , 767.49696, found: 767.49715.

2-O-Arachidonyl-1-O-(3'(4''-pentyn-1''-yl)-H-diazirine-3'-octanoyl)-sn-glycerol (10)



A solution of **9** (96 mg, 131  $\mu$ mol, 1.0 eq.) in DCM (3 ml) was treated with 20% TFA in DCM (3 ml) at 0 °C. The reaction mixture was stirred for 3 min and then poured into saturated Na<sub>2</sub>CO<sub>3</sub> solution (100 ml). The mixture was diluted with EtOAc (100 ml) and the layers were separated. The organic layer was washed with brine (100 ml) and dried over Na<sub>2</sub>SO<sub>4</sub>. The solvent was removed under reduced pressure and the residue was purified by repeated FC (1. eluent: CyHex/EtOAc 4:1; 2. Eluent DCM/acetone 97:3) and the title compound obtained as colorless oil (56 mg, 92  $\mu$ mol, 70 %).

<sup>1</sup>H NMR (400 MHz, CDCl<sub>3</sub>)  $\delta$  = 5.46 – 5.30 (m, 8H), 5.09 (p,  $J$ =4.9, 1H), 4.32 (dd,  $J$ =11.9, 4.6, 1H), 4.28 – 4.19 (m, 2H), 3.77 – 3.67 (m, 2H), 2.88 – 2.76 (m, 6H), 2.41 – 2.28 (m, 4H), 2.21 – 2.01 (m, 6H), 1.95 (t,  $J$ =2.6, 1H), 1.77 – 1.67 (m, 2H), 1.65 – 1.54 (m, 4H), 1.52 – 1.45 (m, 2H), 1.41 – 1.18 (m, 16H), 1.13 – 1.02 (m, 2H), 0.89 (t,  $J$ =6.7, 3H).

<sup>13</sup>C NMR (101 MHz, CDCl<sub>3</sub>)  $\delta$  = 173.74, 173.16, 130.53, 129.03, 128.78, 128.63, 128.32, 128.10, 127.84, 127.53, 72.19, 68.89, 61.98, 61.53, 34.04, 33.64, 32.83, 31.83, 31.53, 29.33, 29.18, 29.11, 29.07, 29.02, 27.23, 26.49, 25.65, 24.81, 24.75, 23.79, 22.75, 22.58, 17.96, 14.08 ppm. Signals at 29.4-29.0 ppm are partially not resolved due to very similar <sup>13</sup>C chemical shifts.

HRMS (m/z): [M+H]<sup>+</sup> calc. for: C<sub>38</sub>H<sub>60</sub>N<sub>2</sub>O<sub>5</sub>, 625.4575; found: 625.4575

### Cell culture

HeLa cells (human cervical adenocarcinoma cells, ATCC/LGC Standards GmbH, No. CCL-2, Wesel, DE) were cultured in DMEM (1g/L glucose, Gibco/Life Technologies) supplemented with 10 % fetal calf serum (Sigma-Aldrich, Lot No.: 032M3395) and 1 % primocin (InvivoGen). Control and NPC human fibroblasts (for genotypes see table below) were obtained from Dr. Forbes D. Porter (NIHCD, Bethesda, USA) and were cultured in DMEM (4.5 g/L glucose, Gibco/Life Technologies) supplemented with 10 % fetal calf serum (Sigma-Aldrich, Lot No.: 032M3395), 2 mM L-glutamine (Gibco/Life Technologies) and 1 % penicillin/streptomycin (Gibco/Life Technologies). All cells were kept in a humidified incubator at 37 °C with 5 % CO<sub>2</sub> and were passaged 2 – 3 times per week.

Cell line	Protein change	cDNA change
<b>NPC17</b>	I1061T, 10bp deletion in exon 19 at codon 962=fs(exon19)	c.3182T>C, c.2884-93delATCACTGACC
<b>NPC22</b>	R978C, IVS21-2 A>G	c.2932C>T, c.3246 – 2A>G
<b>NPC25</b>	fs(exon20), N701K	c.2979dupA   C2103C>G

### Sph uncaging

HeLa cells in 8-well Labteks at 70 – 80 % confluency were labelled with 100  $\mu$ L of 5  $\mu$ M Fluo4 AM (Molecular Probes) solution in imaging buffer (20 mM HEPES, 115 mM NaCl, 1.8 mM  $\text{CaCl}_2$ , 1.2 mM  $\text{MgCl}_2$ , 1.2 mM  $\text{K}_2\text{HPO}_4$  and 0.2 % (w/v) glucose) at 37 °C for 30 min. 15 min prior to the start of the experiment, caged Sph, caged dhSph or trifunctional Sph **1** were added to a final concentration of 2  $\mu$ M. The cells were then washed and kept in imaging buffer at 37 °C for the duration of the experiment.

The fluorescence of the calcium indicator Fluo4 was monitored on a dual scanner confocal laser scanning microscope (Olympus FluoView 1200) using a 63x oil objective at 488 nm excitation and emission settings between 500 - 550 nm at an interval of 1 s per frame. A baseline of 10 frames (= 10 s) was captured before photoactivation ('uncaging') in a circular region (10 pixel units diameter, 8.9  $\mu\text{m}^2$ ) inside the cells using the tornado function of the Olympus software. Coumarin-uncaging was carried out using the 405 nm laser line set to 50 % intensity for 3 s at 2  $\mu$ s per pixel. The time lapse images were analyzed using Fiji software (W. Rasband, NIH, USA) with the FluoQ macro (41) set to the following parameters:

Background subtraction method: Mean of an interactively selected ROI

Noise reduction / smoothing method: None

Threshold method: Interactively with ImageJ's built-in threshold window

ROI segmentation: Semi-automatically with binary mask modification

Calculate amplitude changes: Using maximum observed amplitude change

The resulting intensity series/amplitude values represent mean values of whole cells and were loaded in R and grouped according to lipids (caged Sph vs TFS). Single cell traces belonging to the same groups were summarized using the R function called summarySE which calculated the mean as well as the standard error of the mean of all traces for every time point. Line and bar graphs were generated using the ggplot2 package (42) in R.

### DAG uncaging

DAG uncaging experiments were carried out using HeLa cells transiently transfected with a C1-GFP fusion protein as DAG biosensor. Cell culture conditions and transfection protocols were identical to those reported earlier (2). Cells were seeded in 8-well Lab-Tek™ dishes and transfected 24 hours prior to uncaging experiments. Confocal time-lapses were acquired using an Olympus FV1200 confocal microscope with a 63x oil objective. Cells were treated with a 100 µM solution of the respective caged DAG (TFDAG or SAG) in glucose (20 mM) containing imaging buffer and allowed to equilibrate at 37 °C for 5-10 min. Suitable clusters of C1-GFP expressing cells were chosen for DAG uncaging to ensure high n numbers. Images were acquired at a frame rate of appr. 7 s/frame using 488 nm excitation light and fluorescence was detected between 500 and 580 nm. Uncaging was performed by scanning the entire field of view with a 405 nm laser set to 40% laser intensity after acquiring a baseline of 10 frames. The cellular responses were monitored for additional 50 frames. A maximum of two movies was acquired per single well to minimize batch effects.

Time lapses were analyzed using the ImageJ macro ‘PM/background ratio-calculator Macro’ reported earlier (23) with plasma membrane width defined at 5 pixels. Single pm/cytosol-ratio traces were copied into an excel file and loaded into R. During this process, traces were manually classified into responding and non-responding cells. Furthermore, single cell traces were normalized by dividing each time point by the average of the first 10 time points (time points before uncaging). Averaged traces of SAG and TFDAG were plotted the ggplot2 packages (42). All responding cells were fitted using the nlsLM function of the ‘minpack.lm’ package in R. The following formula was used to fit each normalized single cell trace:

$$DAG_{PM} = 1 + [DAG_{ex}] \frac{-k_{acc}}{k_{met} - k_{acc}} (e^{-k_{acc}t} - e^{-k_{met}t})$$

$k_{acc}$ : accumulation rate constant

$k_{met}$ : apparent metabolism rate constant

$DAG_{ex}$ : height of the trace

As a quality criterion, fits were only used for the statistical analysis if the metabolism constant was above zero and the average difference between the fit and the original values was found to be below 0.06.

### Thin-layer chromatographic analysis of trifunctional lipids

HeLa cells were grown in 60 cm dishes to 85 – 95 % confluency and labelled with 3 µM TFS or 50 µM TFDAG for the indicated times. After washing with PBS, the dishes were transferred onto an ice block and UV-irradiated using a 450 – 1000 W high-pressure mercury lamp

(Newport, USA) equipped with a 400 nm highpass filter for 2.5 min. The cells were washed again and scraped in 300  $\mu$ L PBS and mixed with 600  $\mu$ L MeOH and 150  $\mu$ L  $\text{CHCl}_3$ . The mixture was vortexed and centrifuged at 14 000 rpm for 3 min and the supernatant was transferred into a new vial. 300  $\mu$ L  $\text{CHCl}_3$  and 600  $\mu$ L acetic acid (0.1 % v/v in water) were added, the mixture was again vortexed and centrifuged (14 000 rpm, 4 min) and the aqueous phase was discarded. The organic phase was dried in a speed-vac at 30 °C for 15 min. The lipids were dissolved in 7  $\mu$ L  $\text{CHCl}_3$  and 30  $\mu$ L click-mixture (5  $\mu$ L 44.5 mM 3-azido-7-hydroxycoumarin, 500  $\mu$ L of 10 mM [acetonitrile] $_4\text{CuBF}_4$  and 2 mL EtOH) was added. The reaction vial was vortexed and incubated in a heating block at 42 °C with no shaking for 3 -4 h until all solvent is condensed under the lid. The tube was then vortexed again and the mixture was applied onto a 10 x 10 cm HPTLC Silica 60 glass plate (VWR) using the automatic Camaq system. TLC plates were developed using  $\text{CHCl}_3/\text{MeOH}/\text{H}_2\text{O}/\text{AcOH}$  65:25:4:1 for 6 cm and then cyclohexane/ethylacetate 1:1 for 9 cm. Lipids containing the fluorescent coumarin group were visualized using a geldoc system.

## **Proteomic screens**

### Cell labelling and crosslinking

HeLa cells were grown in three 10 cm dishes for each condition and labelled with 4 mL of 100  $\mu$ M TFFA for 15 min, 100  $\mu$ M TFDAG for 15 min and 6  $\mu$ M TFS probe for 5 min. The cells were then UV-irradiated for 2.5 min at wavelengths above 400 nm followed by a second irradiation at wavelengths above 345 nm and washed with ice-cold PBS. The cells were scraped off in 2 mL PBS and centrifuged at 3000 rpm for 10 min at 4 °C. The cell pellet was resuspended in 300  $\mu$ L PBS, 600  $\mu$ L MeOH and 150  $\mu$ L  $\text{CHCl}_3$  were added, vortexed and centrifuged at 14 000 rpm for 3 min. The protein pellet was resuspended in 100  $\mu$ L PBS and 100  $\mu$ L lysis buffer were added, and shaken at 95 °C for 5 min. After cooling down, 2  $\mu$ L benzonase was added and incubated for 30 min at 37 °C. Next, 100  $\mu$ L of 200 mM DTT (in 200 mM HEPES) was added and incubated at 45 °C for 30 min and then 20  $\mu$ L of 400 mM iodoacetamide (in 200 mM HEPES) was added and shaken at 24 °C for 30 min. Finally, 20  $\mu$ L 200 mM DTT were added to quench the reaction. The proteins were precipitated by addition of 600  $\mu$ L MeOH and 150  $\mu$ L  $\text{CHCl}_3$  and resuspended in 152.5  $\mu$ L PBS/1 % (w/v) SDS/2x PIC by shaking at 37 °C for >1 h. 5  $\mu$ L of the solution was removed for protein determination, the three lysates belonging to the same condition were pooled and stored at - 20 °C.

### Protein determination using Amido Black

A serial dilution of BSA was prepared with 0, 2.5, 5, 7.5, 10, 25 and 50  $\mu$ g BSA in 100  $\mu$ L water. The samples were diluted to 100  $\mu$ L. To all samples, 400  $\mu$ L amido black solution was added, vortexed, incubated at room temperature for 5 min and centrifuged at 14 000 rpm for

5 min. The supernatant was aspirated and the pellets were washed twice with 500  $\mu$ L MeOH/AcOH 10/1. The pellets were dissolved in 300  $\mu$ L 0.1 N NaOH and 150  $\mu$ L were spotted onto a 96 well plate. The absorbance at 550 nm was recorded on a Synergy 4 microplate reader (BioTek, Winooski, USA).

#### Biotinylation and pull-down

The volume of the lysate was adjusted to 1 mg of protein and diluted to 630  $\mu$ L. 30  $\mu$ L of each reagent for click reaction (2.5 mM TBTA in DMSO, 25 mM CuSO<sub>4</sub> in water, 25 mM biotin azide in water, 25 mM ascorbic acid in water) was added and the mixture was shaken at 37 °C for > 3 h. The proteins were precipitated twice using CHCl<sub>3</sub>/MeOH (1:4), redissolved in 160  $\mu$ L PBS/1 % SDS and diluted with 240  $\mu$ L PBS to reach a final SDS concentration of 0.4 % (w/v). After centrifugation at 1000 rpm for 3 min, the supernatant was transferred into a new vial and mixed with 10  $\mu$ L NeutrAvidin agarose resin (Thermo Scientific), which were previously washed three times with 180  $\mu$ L PBS/0.2 % SDS. The lysate was incubated with the resin for 1 h at room temperature and the supernatant was removed. The resin was washed 15 times with PBS/1 % SDS and the proteins were eluted with 50  $\mu$ L elution buffer (100 mM Tris pH 6.8, 4 % SDS, 4 %  $\beta$ -mercaptoethanol) at room temperature for 1 h. The supernatant was taken after heating to 95 °C for 30 min.

#### On-bead tryptic digest (adapted from Hughes et al. (24))

20  $\mu$ L of hydrophilic and hydrophobic Sera-Mag Speed beads (Thermo Scientific) were mixed and kept in 100  $\mu$ L water. The protein lysate was mixed with 5  $\mu$ L formic acid (5 % (v/v) in water) and 5  $\mu$ L beads. Acetonitrile was added immediately to a final concentration of greater than 50 %. The mixture was incubated 8 min at room temperature and was then placed on a magnetic rack for further 2 min. The supernatant was removed and discarded. The beads were washed twice with 200  $\mu$ L EtOH (70 % (v/v) in water) and once with 180  $\mu$ L acetonitrile. The dry beads were then reconstituted in 10  $\mu$ L digestion solution (50 mM HEPES pH 8.0 + 1  $\mu$ g trypsin/LysC (Promega, mass spec grade)) and incubated for 14 h at 37 °C. The peptides were recovered by adding 190  $\mu$ L acetonitrile to the beads, incubating at room temperature for 8 min and for further 2 min on the magnetic rack. The supernatant was removed and discarded. The beads were washed with 180  $\mu$ L acetonitrile and 200  $\mu$ L EtOH (90 % (v/v) in water). Beads were reconstituted in 9  $\mu$ L DMSO (4 % (v/v) in water) and sonicated for 5 min. The supernatant was removed and transferred to a deactivated glass vial containing 1  $\mu$ L formic acid (10 % (v/v) in water).

#### High pH reverse phase offline fractionation (adapted from Bock et al. (43))

The peptide mixture was basified by addition of 10  $\mu$ L 200 mM NH<sub>4</sub>OH and 2  $\mu$ L ammonium formate and injected into an Agilent 1200 Infinity high-performance liquid chromatography (HPLC) system equipped with a peltier-cooled autosampler and fraction collector (both set at 10 °C for all samples). The column was a Gemini C18 column (3  $\mu$ m, 110 Å, 100 x 1.0 mm,



Phenomenex) with a Gemini C18, 4 x 2.0 mm SecurityGuardcartridge (Phenomenex) as a guard column. The solvent system consisted of two mobile phases: Phase A was 20 mM ammonium formate (pH 10.0) and phase B was acetonitrile (100 %). Separation was achieved at a flow rate of 0.1 mL/min using the following linear gradient: 100 % A for 2 min., from 100 % A to 35 % B in 59 min., 100 % A and re-equilibration for 13 min. Thirty-two fractions were collected, which were then non-sequentially pooled into 10 fractions and dried under vacuum centrifugation and reconstituted in 10  $\mu$ L 0.1 % formic acid.

#### Peptide cleanup and enrichment

An Oasis HLB microelution plate (Waters) was washed twice with 200  $\mu$ L 80 % acetonitrile/0.05 % formic acid and then equilibrated twice with 200  $\mu$ L formic acid (0.05 % (v/v) in water) per well. The samples were loaded and the flowthrough was discarded. Samples were then washed twice with 200  $\mu$ L formic acid (0.05 % (v/v) in water). Elution was achieved with 50  $\mu$ L 80 % acetonitrile/0.05 % formic acid. The eluate was dried under vacuum centrifugation and reconstituted in DMSO (4 % (v/v) in water) + 1 % formic acid.

#### LC-MS/MS

Peptides were separated using the nanoAcquity UPLC system (Waters) fitted with a trapping (nanoAcquity Symmetry C18, 5  $\mu$ m, 180  $\mu$ m x 20 mm) and an analytical column (nanoAcquity BEH C18, 1.7  $\mu$ m, 75  $\mu$ m x 200 mm). The outlet of the analytical column was coupled directly to an LTQ OrbitrapVelos Pro (Thermo Fisher Scientific) using the Proxeonnanospray source. Solvent A was water, 0.1 % formic acid and solvent B was acetonitrile/0.1% formic acid. The samples (7  $\mu$ L) were loaded with a constant flow of solvent A at 5  $\mu$ L/min onto the trapping column. Trapping time was 6 minutes. Peptides were eluted via the analytical column a constant flow of 0.3  $\mu$ L/min. During the elution step, the percentage of solvent B increased in a linear fashion from 3 % to 7 % in 10 min, then increased to 25 % in 20 min and finally to 40 % in a further 10 min. The peptides were introduced into the mass spectrometer via a Pico-Tip Emitter 360  $\mu$ m OD x 20  $\mu$ m ID; A 10  $\mu$ m tip (New Objective) and a spray voltage of 2.2 kV were applied. The capillary temperature was set at 300 °C. Full scan MS spectra with mass range 300-1700  $m/z$  were acquired in profile mode in the FT with resolution of 30 000. The filling time was set at maximum of 500 ms with limitation of  $10^6$  ions. The most intense ions (up to 15) from the full scan MS were selected for fragmentation in the LTQ. Normalized collision energy of 40 % was used, and the fragmentation was performed after accumulation of  $3 \times 10^4$  ions or after filling time of 100 ms for each precursor ion (whichever occurred first). MS/MS data were acquired in centroid mode. Only multiply charged ( $2^+$ ,  $3^+$ ,  $4^+$ ) precursor ions were selected for MS/MS. The dynamic exclusion list was restricted to 500 entries with a maximum retention period of 30 s and relative mass window of 10 ppm. In order to improve the mass accuracy, a lock mass correction using a background ion ( $m/z$  445.12003) was applied.

### Data analysis

Proteome Discoverer 1.4 (version 1.4.1.14, Thermo Scientific) was used as raw data post-processing interface with the possibility to select scan events for peptide/protein identification. Identification was performed using a species specific Uniprot database (Homo sapiens taxonomy, 2012, 86945 entries). Mascot (version 2.2.07, Matrix Sciences, London) was used as search engine. Variable amino acid modification was oxidized methionine. Carbamidomethylation of cysteines was set as fixed modification. Trypsin was selected as the enzyme, with one potential missed cleavage. Peptide and fragment ion tolerance was respectively 10 ppm and 0.5 Da. False Discovery Rates (FDR) of 5% (relaxed) and 1% (strict), validated based on q-value, were calculated by Proteome Discoverer based on the search against the corresponding randomized database. Results were filtered on upload for only high peptide confidence, peptide length greater than 6 amino acids and a minimum mascot peptide ion score of 20. The resulting table was read by R, sorted according to peptide spectral match ratios of TFS and TFDAG over control lipids, respectively and visualized as a heatmap by using the ggplot2 package (42). To generate Figure 3b, the GO-term annotations of putative TFS-binding proteins (top 60 hits) and TFDAG-binding proteins (bottom 129 hits) were retrieved from the ensemble database using the biomaRt package (44) for R.

### **Visualization of protein-lipid complexes in cells**

Cells were seeded onto 11 mm coverslips placed in wells of a 24-well plate and labelled with 3  $\mu$ M TFS or 50  $\mu$ MTFDAG or TFFA in imaging buffer for 10 min. Cells were washed, overlaid with 1 mL imaging buffer and UV-irradiated on ice for 2.5 min at wavelengths > 400 nm and for further 2.5 min at wavelengths of > 355 nm. Cells were immediately fixed with MeOH at -20°C for 20 min. Non-crosslinked lipids were extracted by washing three times with 1 mL of CHCl<sub>3</sub>/MeOH/AcOH 10:55:0.75 (v/v) at RT. Cells were then incubated with 50  $\mu$ l of click mixture (1 mM ascorbic acid, 100  $\mu$ M TBTA, 1 mM CuSO<sub>4</sub> and 2  $\mu$ M Alexa 488 azide in PBS) for 1 h at RT in the dark. Cells were then washed with PBS and incubated with 50  $\mu$ l of primary antibody (rabbit  $\alpha$ -LAMP1, Cell Signaling, 1:100, mouse  $\alpha$ -GM130, abcam, 1:200 and rabbit  $\alpha$ -p72, ThermoFisher, 1:100 in PBS supplemented with 4 % BSA and 0.02 % Triton) overnight at 4°C. Coverslips were again washed in PBS and incubated with secondary antibody ( $\alpha$ -rabbit conjugated to AlexaFluor555,  $\alpha$ -mouse conjugated to AlexaFluor555, Cell Signaling, 1:800) for 1 h, washed and mounted in DAPI-containing mounting medium (Vectashield, Vector Laboratories). Microscopy images were captured at room temperature using a confocal laser scanning microscope (Zeiss LSM780) with a 63x oil objective. Settings were as follows: DAPI-channel: 405 nm excitation (ex), 409 - 475 nm emission (em); green channel: 488 nm ex, 489 - 550 nm em; red channel: 561 nm ex, 569 - 655 nm em. Images were further processed

using Fiji software (<http://fiji.sc/Fiji>). The Skewness value for analysis of pixel distribution within cells was directly extracted from the raw images by ticking the Skewness check box in Analyze > Set Measurements ..

### **Visualization of Sph via correlated light- and electron microscopy**

NPC patient cells were seeded on carbon coated Sapphire discs (3mm diameter, thickness 0.05 mm, Engineering Office M. Wohlwend GmbH, Sennwald, Switzerland) for 24 h. Uncaging and crosslinking was performed as described. Cells were then fixed in 4 % PFA in PHEM buffer for 10 min and permeabilized with 0.001 % saponin in PHEM buffer for 5 min before click reaction for 1 h in the dark. The samples were processed within 1 h for high-pressure freezing (HPF) using the HPM 010 (Bal-Tec), placed between two aluminium carriers and a gold slot grid spacer (Plano GmbH, Wetzlar, Germany).

The freeze substitution was performed in a temper temperature-controlling device (AFS2, Leica) in acetone supplemented with 0.1 % (w/v) uranyl acetate for 24 h at -90 °C (45, 46). The temperature was raised to -45 °C within 10 h, held at that temperature, washed three times with acetone and infiltrated by Lowicryl HM20 (Polysciences Europe GmbH, Eppelheim, Germany) for 4 h periods at increasing concentrations (10 %, 25 %, 50 %, 75 %). The temperature was subsequently raised to -25 °C (5 °C/hour) and the final Lowicryl concentration of 100 % was held and washed every 10 h for three times. The blocks were finally polymerized by UV light incubation for 48 h at 20 °C.

Thick sections (300 nm) were cut using a Leica Ultracut UCT microtome mounted with a diamond knife (Diatome, Biel, Switzerland). Each section was placed on a carbon-coated copper grid (Plano GmbH, Wetzlar, Germany), incubated for 8 min in a drop of 1:200 with 50 nm fluorescent microspheres in PBS (TetraSpecks, Life Technologies) followed by 3 times washing in water. The grids were sandwiched between two coverslips (Menzel-Gläser, No. 1) filled with 30 µL water and sealed by vacuum grease. Samples were imaged using a Metamorph (Molecular Devices) operated wide-field fluorescence microscope (Olympus IX81) equipped with an X-Cite 120PC light source (EXFO Life 2 Sciences), an Olympus PlanApo 100x 1.45 NA oil immersion objective, Orca-ER camera (Hamamatsu Photonics), electronic shutters and filter wheels (Sutter Instruments Co.). 470/22 nm and 556/20 nm excitation filters were used in combination with emission filters 520/35 nm for Tetraspecks and 624/40 nm for Alexa594.

The grids were incubated with gold fiducial markers (15 nm) and placed into a single-tilt holder on a Tecnai TF30 microscope (FEI) at 300 kV using Serial EM for electron tomography (37). Images were acquired at -60 to +60 ° (1 ° increment) recorded by a 4K Eagle camera (FEI) at a pixel size of 5.068 nm and reconstructed using IMOD (versions 4.1.4) (47). Fluorescent and

electron tomography images were correlated based on the fluorescent and gold fiducials using a MATLAB script.

**Figure S1:** TFS and TFDAG metabolism in cells by thin-layer chromatography (TLC). a)/c) HeLa cells were labelled with 3  $\mu$ M TFS (a) or 50  $\mu$ M TFDAG (c) for the indicated times without UV irradiation. Cellular lipids were extracted, labelled with 3-azido-7-hydroxycoumarin by click reaction and separated on a TLC plate. b)/d) HeLa cells were labelled with 3  $\mu$ M TFS (b) or 50  $\mu$ M TFDAG (d) for 15 min, washed and irradiated with >400 nm UV light for 2.5 min and incubated for the indicated times. Cellular lipids were extracted, labelled with 3-azido-7-hydroxycoumarin by click reaction and separated on a TLC plate.

**Figure S2:** Individual traces of C1-GFP translocation. The fluorescence ratio of C1-GFP at the plasma membrane and the cytosol was recorded for HeLa cells treated with 100  $\mu$ M caged SAG and 100  $\mu$ M TFDAG, respectively. Uncaging was carried out by scanning the entire field of view as indicated by the arrow. Cells were then classified into responder and non-responder (gray traces).

**Figure S3:** Individual, fitted C1-GFP translocation traces for cells that matched the quality control test. Each cell was fitted with a biexponential model (see SI Materials and Methods). The resulting half-times of DAG metabolism are displayed in seconds next to the traces.

**Figure S4:** Subcellular distribution of trifunctional lipids. Confocal images of HeLa cells incubated with the indicated concentrations of trifunctional lipids.

**Figure S5:** a) Overlap of TFS-interactors with previous screens. Proteins identified as unique interactors using TFS were compared to proteins identified in a previous screen using pacSph as bait (20). The spectral counts of proteins which were either not present in the previous screen (not previously identified, left column), identified with pacSph (pacSph, top right column) or pacFA only (pacFA, middle right column) or identified with both pacFA and pacSph (pacFA/pacSph, bottom right column) are displayed using the same color code as in Figure 3. b) Overlap of TFDAG-interactors with previous screens. Proteins identified as unique interactors using TFDAG were compared to proteins identified in a previous screen using arachidonic acid-containing lipids in HEK293-T cells (21). The spectral counts of proteins which were either not present in the previous screen (not previously identified, left columns), identified with AEA-DA (AEA-DA, centre column), A-DA (A-DA, middle right column) or identified with both AEA-DA and A-DA (AEA-DA/A-DA, bottom left column) are displayed using the same colour code as in Figure 3.

**Figure S6:** Subcellular localization of trifunctional lipids. a) Confocal images of HeLa cells treated with 6  $\mu$ M TFS for 5 min, 100  $\mu$ M TFDAG or 100  $\mu$ M TFFA for 15 min, respectively. The top panel shows lipid localization before uncaging as visualized by coumarin-fluorescence. Uncaged, crosslinked and fixed lipids are visualized using Alexa488-azide and are shown in the bottom panel. b) Quantification of total fluorescence intensity of Alexa488-labelled TFS, TFDAG and TFFA, respectively. c) Confocal images of HeLa cells treated with 6  $\mu$ M TFS and 100  $\mu$ M TFDAG, respectively. Alexa488-azide-conjugated lipids are shown in gray (left hand side) and green (merged image). Late endosomes/lysosomes were stained using LAMP1 antibody and are displayed in gray (middle image) and red (merged image). The scale bars represent 20  $\mu$ m. d) Quantification of fluorescence intensity in lysosomes. LAMP1 immunofluorescence was used to identify regions that mark lysosomes. The combined integrated density of these regions in the lipid channel was divided by the integrated density of the whole cell to obtain the ratio displayed on the y-axis. e) and f) Confocal images of HeLa cells treated with 6  $\mu$ M TFS and 100  $\mu$ M TFDAG, respectively. Alexa488-azide-conjugated lipids are shown in gray (left hand side) and green (merged image). Golgi apparatus and ER

were stained using GM130 and p72 antibody, respectively and are displayed in gray (middle image) and red (merged image). The scale bars represent 20  $\mu\text{m}$ .

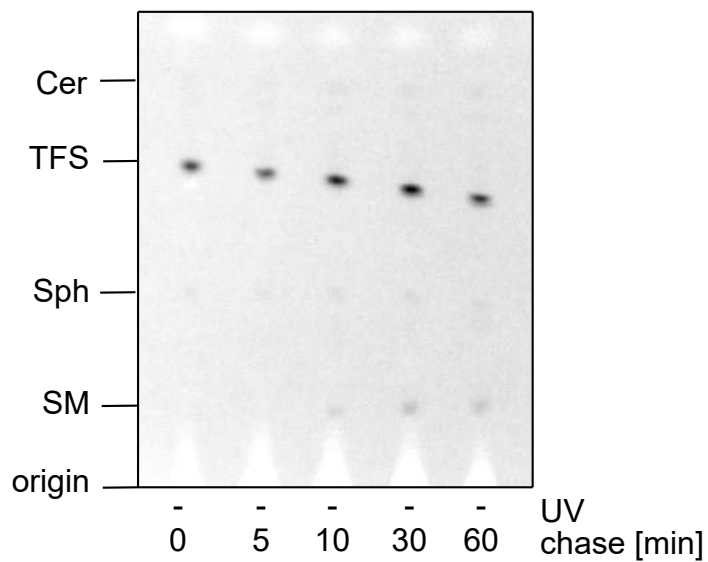
**Figure S7:** a) Filipin staining of HeLa cell models of NPC. Confocal images of HeLa cells treated with U18666A (2  $\mu\text{g}/\text{mL}$  for 24 h) or siRNA against NPC1. Cells were fixed with PFA and stained using Filipin complex (from *S. aureus*, 50  $\mu\text{g}/\text{mL}$ ). b) TFS co-localization with endosomes/lysosomes in NPC cell models. Confocal images of HeLa cells treated with U18666A (2  $\mu\text{g}/\text{mL}$  for 24 h) or siRNA against NPC1. 6  $\mu\text{M}$  TFS was added for 5 min, the cells were washed and subsequently uncaged and crosslinked. The time between uncaging and crosslinking was varied from 0 min to 30 min. Cells were fixed, washed and the crosslinked lipids were functionalized with Alexa488. Late endosomes/lysosomes are visualized via LAMP1 antibody in grey (middle image) and red (merged image) and Pearson's correlation coefficient is shown in the top left corner of the merged image. The scale bars represent 20  $\mu\text{m}$ .

**Supporting Movie M1:** Time-lapse video of HeLa cells expressing C1-GFP, treated with 100  $\mu\text{M}$  of TFDAG and uncaged by scanning the entire field of view with a 405 nm laser once at  $t=60$  s.

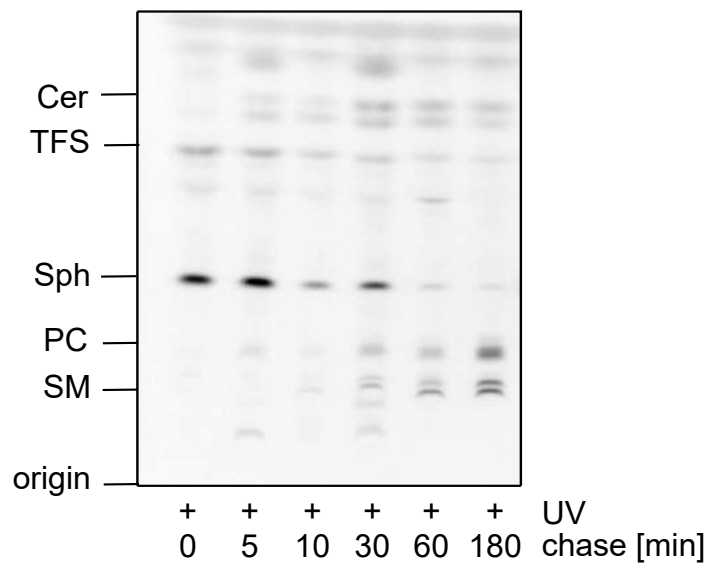
**Supporting Movie M2:** Time-lapse video of HeLa cells expressing C1-GFP, treated with 100  $\mu\text{M}$  of caged SAG and uncaged by scanning the entire field of view with a 405 nm laser once at  $t=60$  s.

**Supporting Table 1:** Hit proteins identified in two independent screens with three lipid probes TFS, TFFA and TFDAG arranged as in Figure 3a with their respective peptide spectral matches (PSM). Proteins only identified with TFS and TFDAG, respectively are displayed in separate sheets.

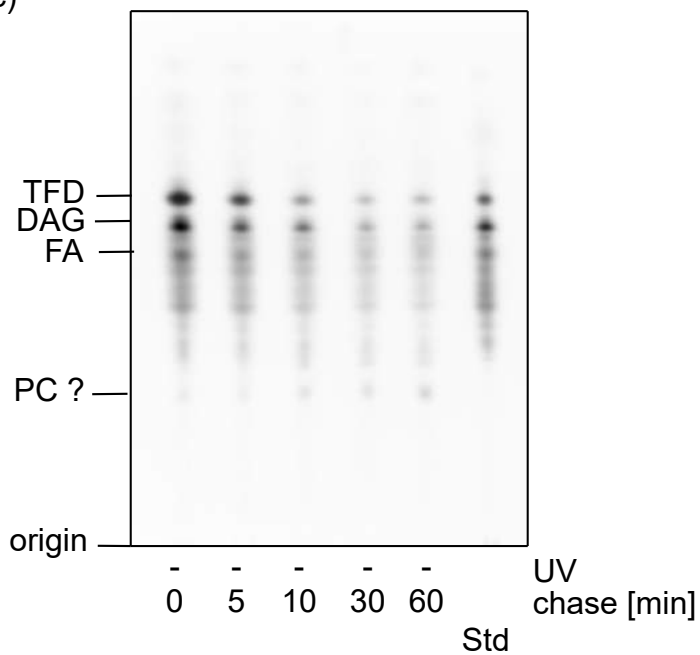
a)



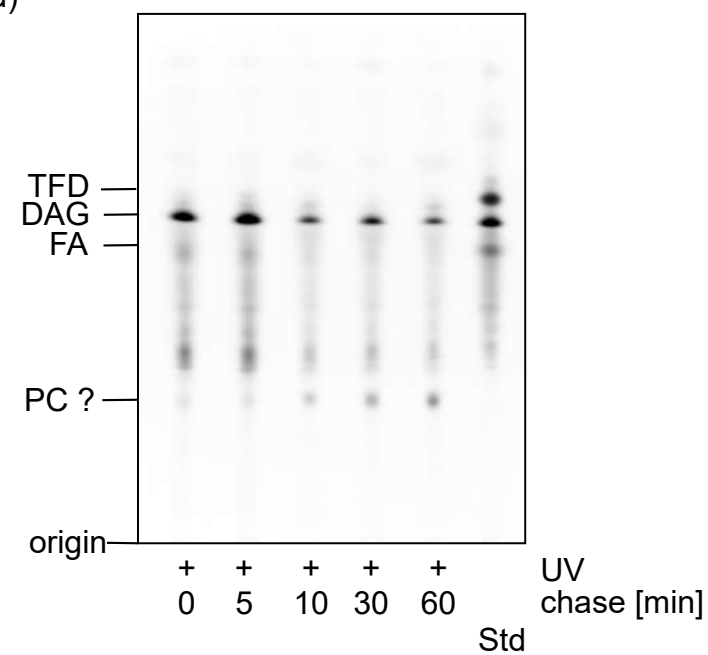
b)

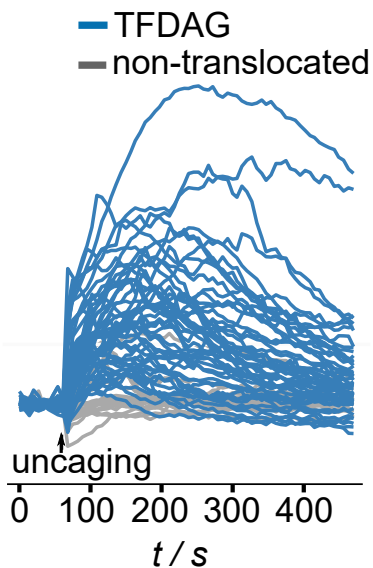
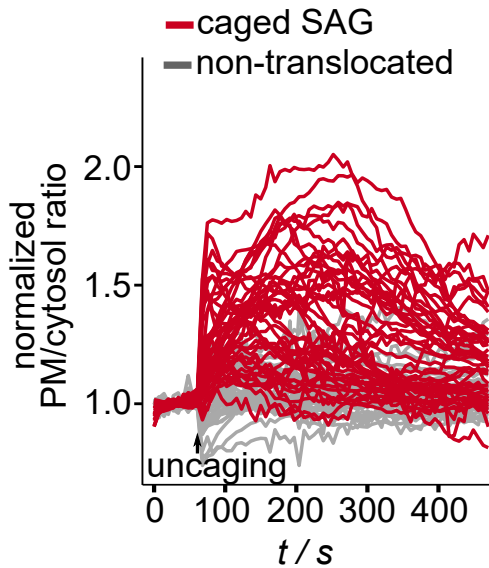


c)

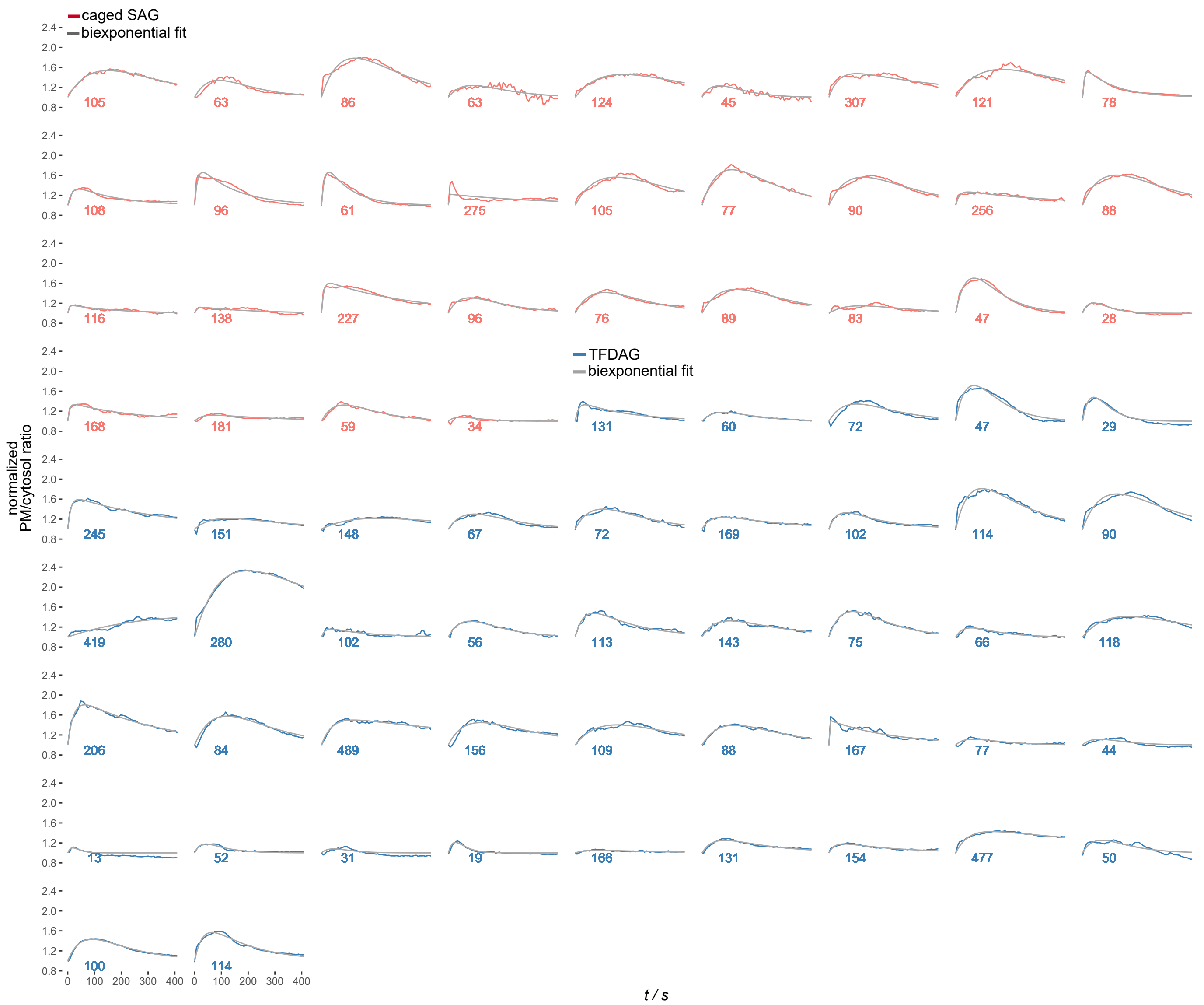


d)





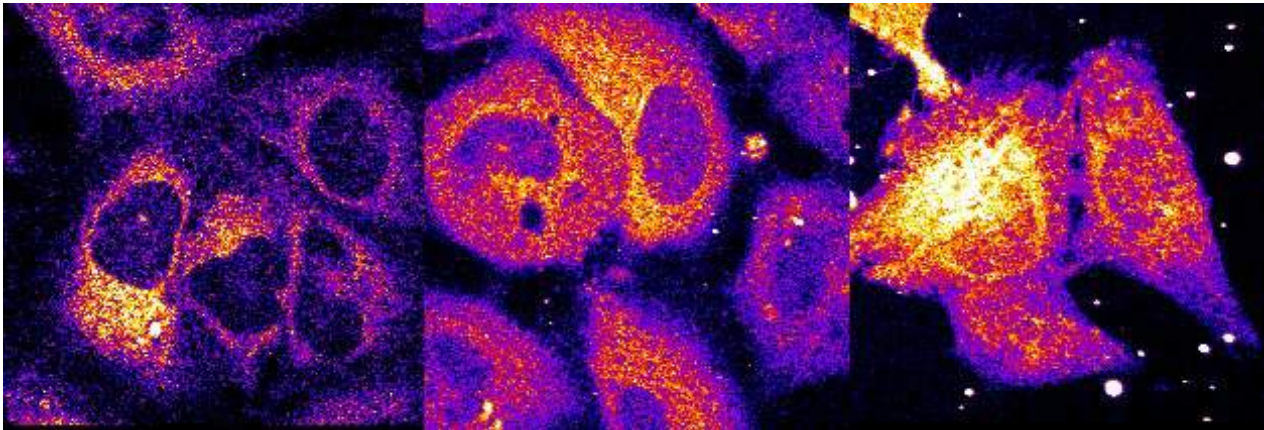




**TFS**

**TFDAG**

**TFFA**



6  $\mu\text{M}$   
5 min

100  $\mu\text{M}$   
15 min

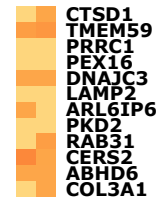
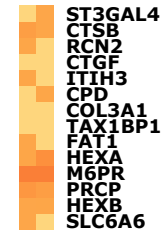
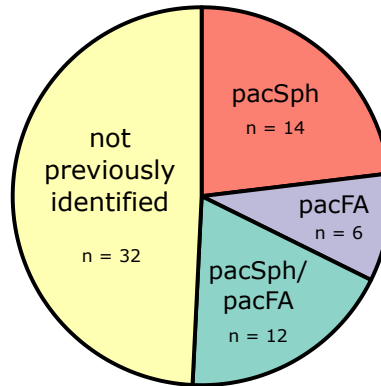
100  $\mu\text{M}$   
15 min

a)

Proteins uniquely identified with TFS

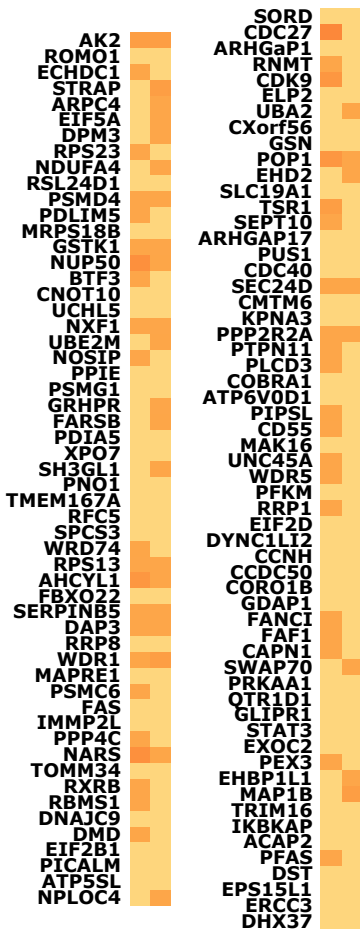


Proteins identified with TFS as well as bifunctional probes pacSph and/or pacFA



b)

Proteins uniquely identified with TFDAG



Proteins identified with TFDAG as well as arachidonic acid containing probes AEA-DA and/or A-DA

